AD_____

Award Number: DAMD17-02-1-0719

TITLE: Interrogating Androgen Receptor Mediated Gene Expression and Tumor Progression by Molecular Imaging

PRINCIPAL INVESTIGATOR: Michael F. Carey

CONTRACTING ORGANIZATION: University of California
Los Angeles, CA 90024-1406

REPORT DATE: October 2003

TYPE OF REPORT: Annual

PREPARED FOR: U.S. Army Medical Research and Materiel Command
Fort Detrick, Maryland 21702-5012

DISTRIBUTION STATEMENT: Approved for Public Release;
Distribution Unlimited

REPORT DOCUMENTATION PAGE

Form Approved
OMB No. 074-0188

1. AGENCY USE ONLY (Leave blank)	2. REPORT DATE	3. REPORT TYPE AND DATES COVERED
	October 2003	Annual (9 Sep 2002 - 8 Sep 2003)

4. TITLE AND SUBTITLE
Interrogating Androgen Receptor Mediated Gene Expression and Tumor Progression by Molecular Imaging

5. FUNDING NUMBERS
DAMD17-02-1-0719

6. AUTHOR(S)
Michael F. Carey

7. PERFORMING ORGANIZATION NAME(S) AND ADDRESS(ES)
University of California
Los Angeles, CA 90024-1406

E-Mail: mcarey@mednet.ucla.edu

8. PERFORMING ORGANIZATION REPORT NUMBER

9. SPONSORING / MONITORING AGENCY NAME(S) AND ADDRESS(ES)
U.S. Army Medical Research and Materiel Command
Fort Detrick, Maryland 21702-5012

10. SPONSORING / MONITORING AGENCY REPORT NUMBER

11. SUPPLEMENTARY NOTES
Original contains color plates: ALL DTIC reproductions will be in black and white

12a. DISTRIBUTION / AVAILABILITY STATEMENT
Approved for Public Release; Distribution Unlimited

12b. DISTRIBUTION CODE

13. ABSTRACT (Maximum 200 Words)

The main goal of the project is to develop a transcription-based optical imaging system for studying androgen receptor (AR) function during prostate cancer progression in animal models. We have now developed a system termed two-step transcriptional activation (TSTA) and used it to show that AR is functional in the androgen independent (AI) phase of the cancer. Mechanistic analyses showed that AR was localized to the nucleus, bound its enhancers and assembled transcription complexes in AI cancers. We have also modified the TSTA system to detect elevated levels of mitogen activated protein kinase (MAPK) in cell culture and in AI animal models of prostate cancer. We are employing the MAPK optical imaging system to study the transition of prostate cancer from androgen dependence to AI. Preliminary data suggest that AI cancer contains markedly elevated levels of MAPK compared with AD cancer.

14. SUBJECT TERMS
Androgen receptor, prostate cancer, MAPK, molecular imaging

15. NUMBER OF PAGES
40

16. PRICE CODE

17. SECURITY CLASSIFICATION OF REPORT	18. SECURITY CLASSIFICATION OF THIS PAGE	19. SECURITY CLASSIFICATION OF ABSTRACT	20. LIMITATION OF ABSTRACT
Unclassified	Unclassified	Unclassified	Unlimited

Table of Contents

Introduction: The goal of our study is to analyze the mechanism of androgen-receptor (AR)-mediated gene activation in androgen-independent (AI) prostate cancer using powerful new technologies: Noninvasive optical imaging, chromatin immunoprecipitation and immobilized template analysis. Our model system is a SCID mouse implanted with a human prostate tumor. The tumor mimics the natural transition of the cancer from the androgen dependent (AD) to AI state upon castration of the animals. Our previous studies have demonstrated our ability to track metastatic lesions and illuminate prostate cancer using gene expression-based imaging cassettes in combination with a charge coupled device (CCD) optical imaging system (refs. 1-5). Our current imaging cassette is termed TSTA or two-step transcriptional activation. In TSTA, a modified PSA enhancer is employed to synthesize GAL4-VP16, which activates luciferase expression to very high levels. An emerging benchmark of advanced prostate cancer progression is elevated mitogen activated protein kinase (MAPK) activity possibly initiated by receptor tyrosine kinase (RTK) signaling (Figure 1)(Reviewed in refs 6-8). This directly or indirectly leads to augmented transcription complex assembly and expression of AR-regulated genes *in vivo*. The mechanism of this effect is largely unknown but probably underlies the development of AI cancer. Our hypothesis is that the MAPK signaling induces modifications of AR function that permit AR to act in a ligand-depleted environment. Our goals was to develop a prostate cancer imaging system to detect augmented MAPK activity in prostate tumors of living animals and correlate it with enhanced AR function.

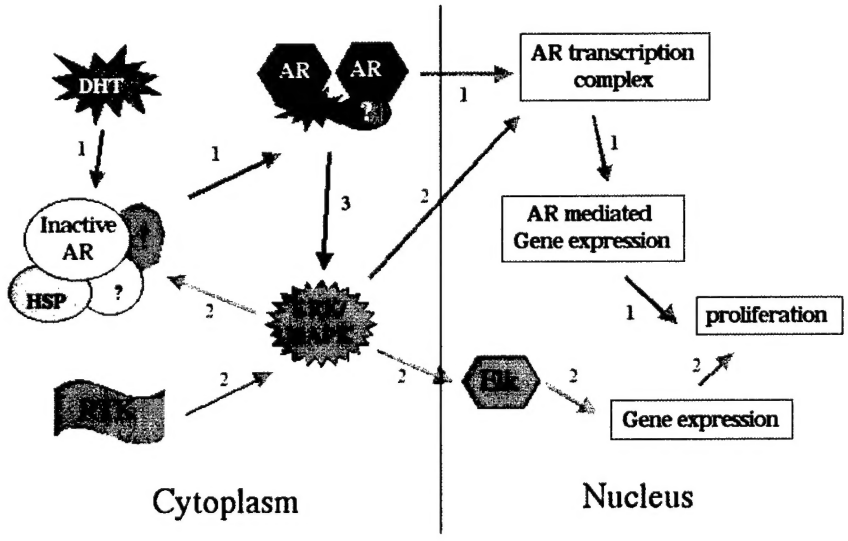

Figure 1 AR-mediated prostate cancer growth: A diagram of proposed mechanisms for AR-regulated gene expression and cell growth. In pathway 1, DHT binds AR, causing dissociation of HSP chaperones, dimerization, nuclear localization, transcription complex assembly, gene activation and cell proliferation. In pathway 2, Receptor tyrosine kinase (RTK)-linked MAPK cascades converge at ERK, which activates Elk-1 and possibly some components of the AR transcription complex. This allows growth of prostate cancer at castrate levels of ligand. An alternative pathway is that MAPKs facilitate response to castrate levels of ligand by acting on the chaperone complex and the nuclear localization of AR. Finally, pathway 3 illustrates a non-genotropic mechanism by which AR activates the MAPK pathway directly

Statement of Work and Results

Task 1: Develop the MAPK-TSTA expression system.

The initial goal of the study was to develop an imaging system that could detect elevated MAPK levels during the transition between the androgen dependent and independent forms of prostate cancer. The basic hypothesis as stated in Figure 1 is that elevated MAPK facilitates the conversion to the AI state. To test the idea that MAPK is elevated in AI cancer we developed a plasmid-based imaging system based on a concept being developed in the lab termed two step transcriptional activation or TSTA.

In the TSTA system (refs. 2-5) we use an androgen receptor (AR)-responsive prostate specific antigen (PSA) enhancer to drive GAL4-VP16. GAL4-VP16 is a potent transcriptional activator and binds to GAL4 recognition sites upstream of a Firefly luciferase reporter gene. When AR is active then GAL4-VP16 is synthesized, binds DNA, and luciferase is expressed. The amount of luciferase is proportional to the amount of AR activity in the cell. We measure luciferase in cell culture by adding D-luciferin and ATP to cell extracts and light is quantitated using standard luminometry. In live animals we inject D-luciferin into the animal and detect luciferase activity using a charge coupled device camera, which quantifies the photons emitted from tissues expressing luciferase in the live animal. The process is not toxic and animals can be imaged repetitively over weeks or months. The system is described in several previous publications from my lab with my collaborators, Drs. Sam Gambhir and Lily Wu (refs. 2-6).

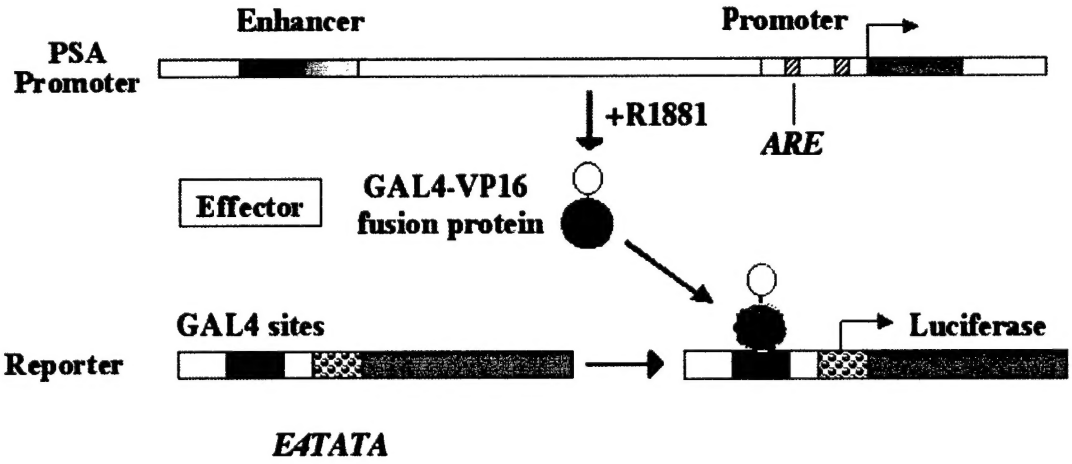

Figure 2. The rationale of Two Step Transcription Activation (TSTA) system. In the first step, the "effector" GAL4-VP16 derivatives (oval circles) are expressed in prostate cancer cells in the presence of androgen (R1881), which activates the PSA enhancer, PSE. In the second step, GAL4-VP16 binds to a GAL4-responsive promoter, and activates expression of the "reporter" firefly luciferase. GAL4: GAL4 DNA Binding Domain. VP16: VP16 activation domain. E4TATA contains the adenovirus E4 minimal promoter.

The most recent publications were supported by the DOD award as they involved a combination of optimizing the TSTA system for use in animals and comparison of AR activity in AD and AI prostate tumors.

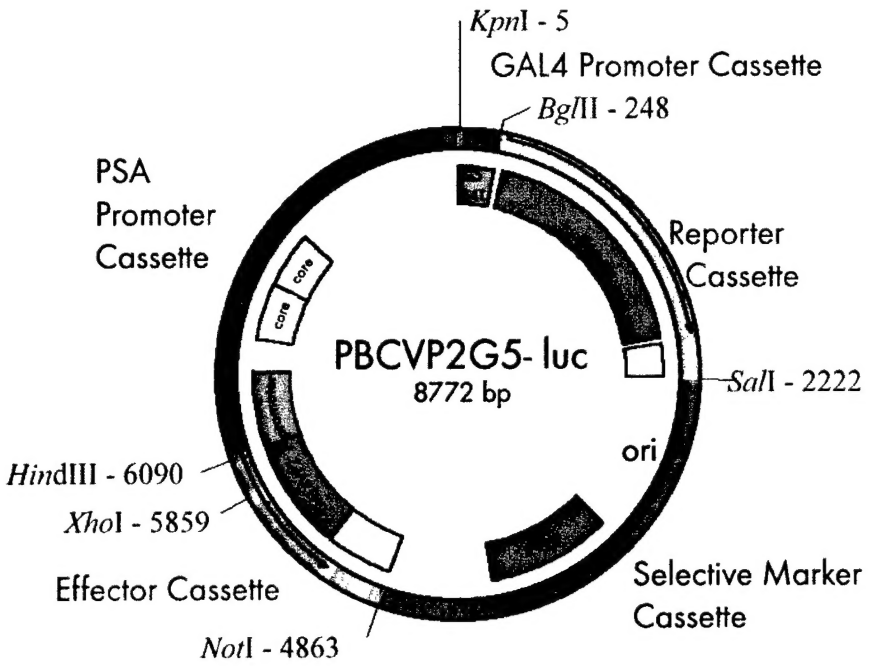

Figure 3. The optimal TSTA system in a single construct This figure illustrates the construct containing the optimal TSTA combination in a "head-to-head" orientation. There are four cassettes. 1. The tissue specific promoter cassette currently containing PBC. 2. The GAL4 activator cassette currently containing GAL4-VP2; 3. The GAL4 site cassette currently containing G5; and 4. The reporter gene cassette bearing FLuc. Each casette is flanked by unique restriction endonuclease sites for swapping the different components and the entire TSTA module can be removed by NotI-SalI digestion for insertion into AdEasy.

The studies involved creating a single plasmid that contained the optimal TSTA system. In the optimal system we duplicated the PSA enhancer to augment the amount of GAL4-VP16 synthesized in the presence of AR. We also duplicated the VP16 activation domain to create GAL4-VP2. This is a more potent activator than GAL4-VP16 and leads to higher levels of firefly luciferase expression. The plasmid also contains unique restriction sites, which we employed to generate the MAPK-responsive system described below. We then inserted the optimal TSTA system into an adenovirus and tested it in cell culture and in SCID mice bearing AD and AI tumors of a prostate cancer model termed LAPC9. The studies are described in the appended paper Zhang et al. (2003). In short, we proved using molecular imaging, chromatin immunoprecipitation and AR localization studies that the AR pathway was fully functional in AI cancer. The work is described further below in Tasks 5 and 6.

We next modified TSTA to measure MAPK activity after having established the activity of AR in the original transcription based TSTA imaging system. We took advantage of the fact that MAPK activates the transcription factor Elk-1 by phosphorylation as stated in Figure 1. By replacing the VP2 activation domain in the plasmid of Figure 3 with the MAPK-responsive transcription activation domain of Elk-1 we generated a single plasmid with the GAL4-Elk-1 gene under control of the PSA enhancer. This plasmid synthesizes firefly luciferase only when both AR and MAPK are active (Figure 4). Thus the amount of luciferase activity is related to the activity of MAPK.

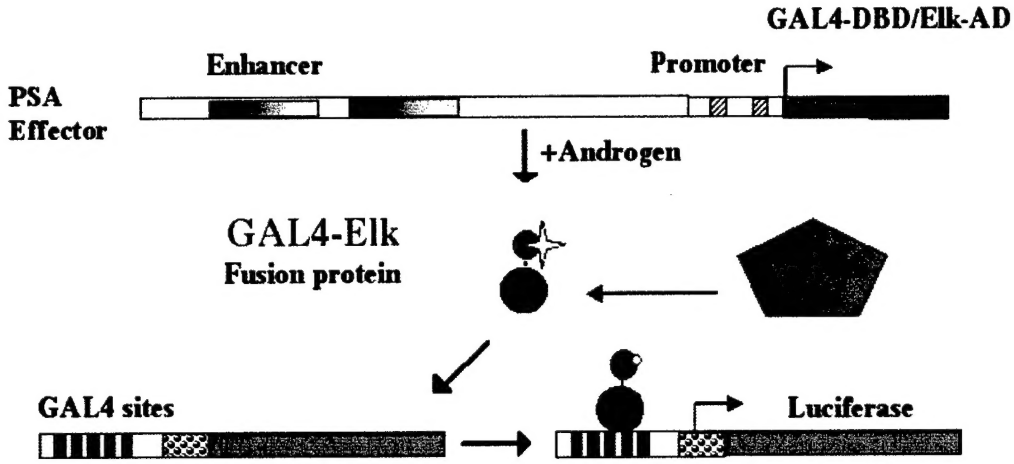

Figure 4. The TSTA-Elk system. The general scheme is the same as in figure 2 but GAL4-VP2 is replaced by GAL4-Elk. GAL4-Elk is only synthesized when AR and the PSA enhancer are active. GAL4-Elk however is only active when MAPK activity is present in tumor cells. MAPK phosphorylates the Elk activation domain (yellow star and circle) allowing it to effect luciferase expression.

This single plasmid TSTA-Elk system was then employed the experiments described in Tasks 2-4. We originally intended to clone the TSTA-Elk system into adenovirus. To this end we have cloned the TSTA-Elk system into an adenovirus shuttle vector and initiated experiments to use the commercial AdEasy system to recombine the cassette into the adenovirus genome. However we found that the plasmid could be introduced into tumor cell suspensions by transfection and that the transfected cells expressed the plasmid for weeks after they were introduced into animals. Because this approach greatly facilitated our analysis we employed it to perform the experiments listed in Tasks 2 and 4. We have therefore temporarily bypassed Task 3 although we have experiments in progress to generate the adenovirus.

Task 2: Testing the MAPK-TSTA system in cell based assays.

The goal of this task was to test for prostate specificity of the TSTA-Elk system in cell lines and to test for response to androgens, MAPK stimuli and pathway inhibitors. This phase of the testing is largely complete. We found that the TSTA-Elk is prostate cell specific, comparable to the results we previously reported for TSTA. I will therefore focus on experiments showing the functionality of TSTA-Elk, which were performed in the prostate cancer cell line LNCaP. LNCaP cells contain AR, express PSA and respond to external MAPK stimuli such as the epidermal growth factor (EGF) pathway. EGF activates MAPK by binding to the EGF receptor (EGFR), which stimulates phosphorylation of the MAPKs ERK1/2. We also performed experiments in cell suspensions derived from AD and AI LAPC9 tumors in SCID mice. LAPC9 AD and AI cells also express AR, PSA and respond to MAPK stimuli. There is a distinct difference between AD and AI cells that I will describe both here and in Task 4.

The most compelling data that prove TSTA-Elk functions as predicted involve transfection of the TSTA-Elk plasmid into LNCaP cells treated with EGF and the

synthetic androgen R1881. To validate the response we also tested the effects of two inhibitors. Casodex is a non steroidal androgen antagonist that binds to AR and inhibits its ability to respond to natural and synthetic androgens (i.e., DHT and R1881). PKI166 is a drug that binds to and inhibits the receptor tyrosine kinase activity of EGFR.

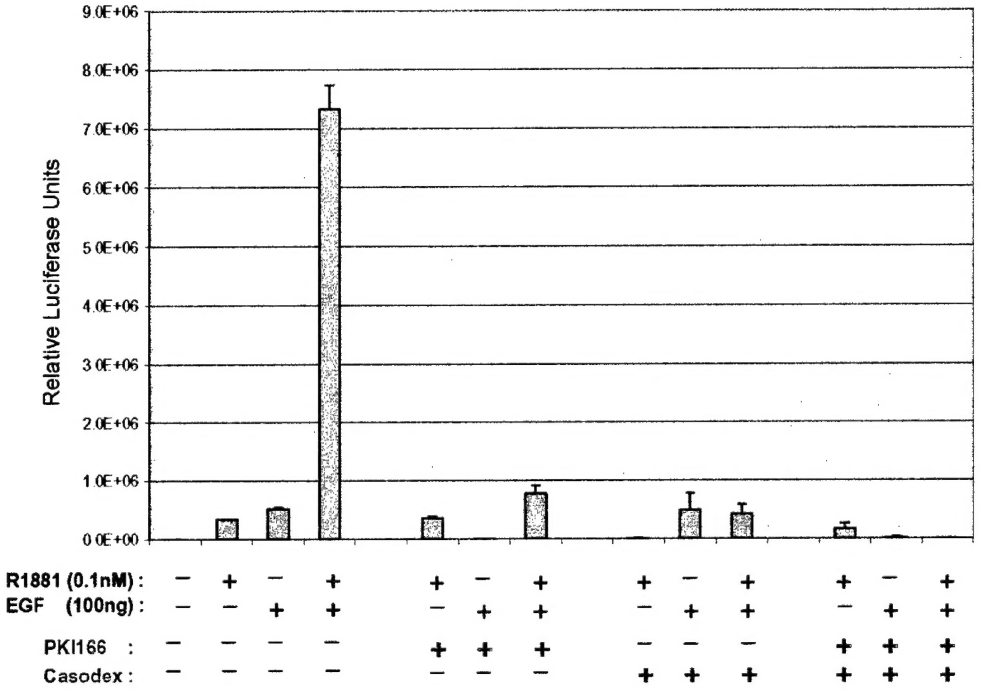

Figure 5. Activity of the TSTA-Elk System in LNCaP cells. TSTA-Elk was transfected into LNCaP cells grown in steroid-depleted medium. The cells were treated with either 0.1 nM R1881 to activate AR, or 100 ng of EGF to activate the MAPK pathway. Casodex at 0.1 mM was added to inhibit AR and PKI166 added at 10 nM was used to inhibit EGF and hence MAPK. Cell extracts were prepared and luciferase activity was measured by luminometry. Experiments were performed in triplicate and standard deviation is indicated on the bars.

Figure 5 is a bar graph of the luciferase activity from LNCaP cells transfected with the TSTA-Elk system. The first 4 bars show that significant luciferase activity is detected only when both R1881 and EGF are added to cells. This result is predicted because R1881 activates AR and hence GAL4-Elk expression. However GAL4-Elk is only fully active when EGF activates MAPK activity. Immunoblot analysis (not shown) confirmed that GAL4-Elk is synthesized in response to R1881

The effects are specific because Casodex lowers AR activity and thus blocks the expression of GAL4-Elk as shown in the next three bars. Further, even though GAL4-Elk is present, PKI166 inhibits activity by blocking EGFR and thus blocks MAPK as shown in the next three bars. Immunoblot analysis was used to confirm that EGF-mediated ERK phosphorylation was inhibited by PKI166.

The last three bars show the combined effect of Casodex and PKI. In short, the results establish conclusively that AR and MAPK are both needed for robust activity of TSTA-Elk in prostate cancer cell lines.

Analysis of the TSTA-Elk system in LAPC9 AD and AI tumor suspensions is still ongoing but the preliminary data allow us to make the following conclusions.

1. TSTA-Elk is relatively inactive in AD but is active in AI cell suspensions derived from tumors.
2. TSTA-Elk responds to EGF in AI cells but not initially in AD cells.
3. Pretreatment of AD cells with EGF facilitates tumor growth in animals and primes the AD cells to respond to EGF as they transition into the AI state (see below)

Task 4: Analyze the AR-MAPK pathway using the TSTA-Elk *in vivo* imaging system. There are several subtasks that relate to the ability of TSTA-Elk to respond to anti-androgens like flutamide and anti-MAPK drugs like PKI166 in live animals. We initially performed these experiments with the TSTA system to evaluate the drug effects on AR in vivo in the context of tumors. This is an essential control for determining the effects of the drugs on TSTA-Elk since AR function is necessary to activate the Elk system. I will review three sets of experiments: The effect of the anti-androgen flutamide on AR function and tumor growth in AD and AI xenografts; the effects of PKI166 on AI tumor growth and TSTA function; and finally the initial data on TSTA-Elk in live animals.

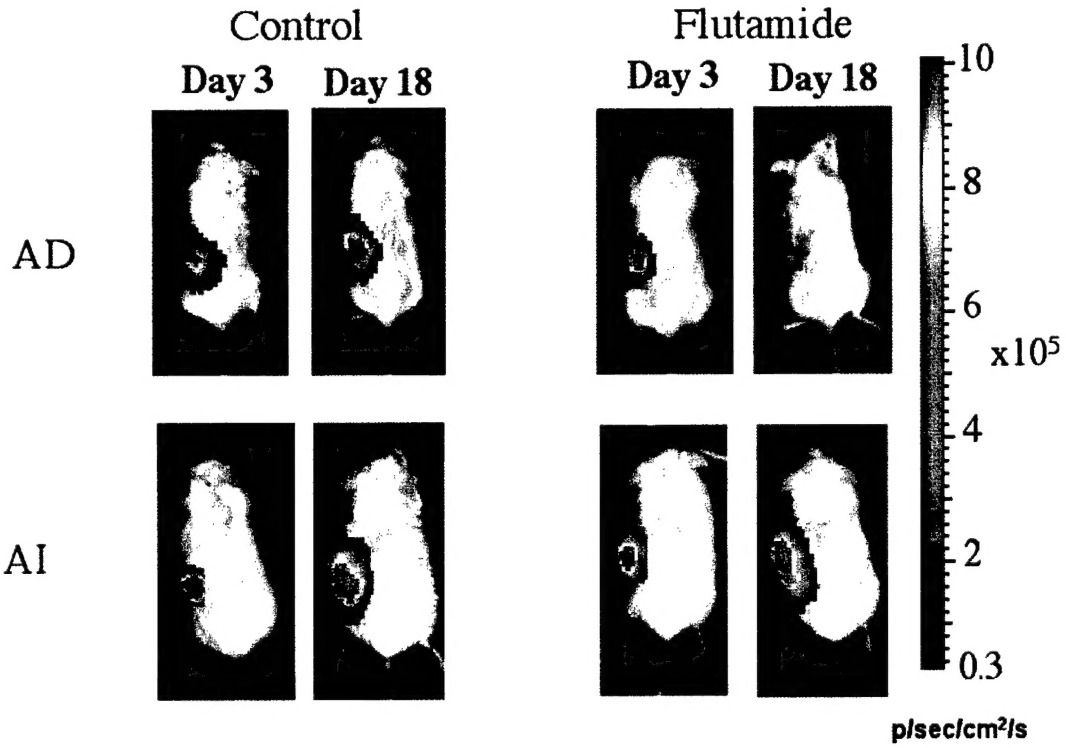

Figure 6. Effect of Flutamide on AdTSTA Activity in Tumors: 10^7 pfu of AdTSTA were injected directly into LAPC9 AD (top panels) and AI (bottom) tumors on day 1. On Day 3 a baseline image of the animals was taken and pellets containing vehicle (control animals, left two panels) alone or the anti-androgen flutamide (right panels) were implanted on the backs of the mice. The animals were imaged using a CCD camera on Day 18 to examine the effects of flutamide on AR activity. The pseudoimage indicates the intensity of the signal. The signal intensity scale in photons/sec/cm^2 of area per steridian is illustrated to the right.

Figure 6 shows that flutamide strongly inhibits the action of AR in vivo in AD but not AI tumors as measured by CCD imaging of live tumor-bearing animals. This is illustrated by comparing the signal on Day 3 to Day 18 in the flutamide treated AD versus AI animals. In the AD animals the signal decreases significantly while in the AI animals the signal actually increases slightly. Similar results were observed in cohorts of three animals and a more extensive study is underway. In Zhang et al. 2003 we discussed the ability of TSTA to respond to androgen depletion by castration of AD animals and proposed how AR escapes the effects of androgen depletion after transition to the AI state. One idea was that the castrated animal somehow compensates by increasing the synthesis of androgen in the tumor. If this was true we would have expected flutamide to inhibit in both AD and AI animals. The inability of flutamide to impact the AR pathway in AI suggested that AR is using a ligand independent mechanism.

We next asked whether the AI tumors are actively using the EGF pathway to stimulate AR function (Figure 7). Our collaborator, Dr. Sawyers provided us with guidance on an animal treatment protocol published in Mellinghoff et al. (2002) (ref. 9). In this case we established tumors bearing an integrated lentivirus construct containing the TSTA cassette described in Figure 3. We implanted the LAPC9 AI tumor cell suspensions infected with Lenti-TSTA into SCID mice and treated by gavage with suspensions of PKI 166 beginning on day 3. We monitored tumor growth and the effect of PKI up to day 18.

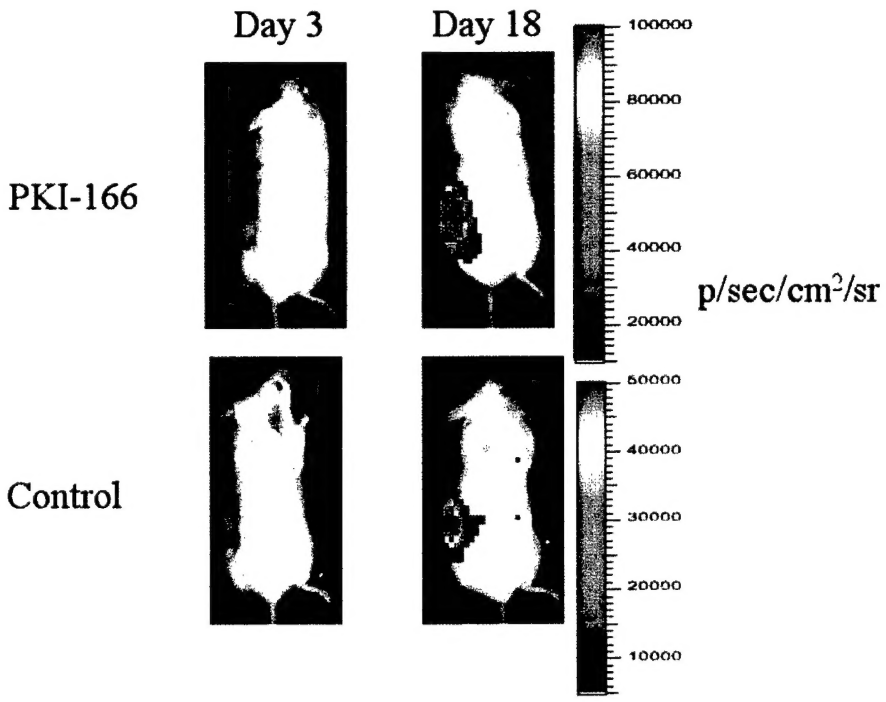

Figure 7. Treatment of LAPC9 AI Tumors with PKI and Monitoring with TSTA. SCID mice bearing LAPC9 AI tumors were treated with PKI beginning 3 days after the tumor cell implantation. CCD imaging was performed on Day 3 after tumor implant and then on Day 18 after a course of PKI166. The imaging scale is shown to the right.

We were surprised to discover that PKI166 did not alter AR signaling since the animals treated with vehicle alone elicited the same signals on Day 18 as PKI166-treated animals (compare top and bottom panels). This result suggested a number of possibilities including that the tumors are simply incapable of responding to PKI166 or that the EGF pathway is not the pathway driving AR activity and cell proliferation in AI tumors.

To establish that the AI cells could actually respond to PKI we performed a cell culture transfection of TSTA-Elk system into LAPC9 AI cell suspensions and tested: i. EGF activity and ii. ability of PKI166 to inhibit it (Figure 8).

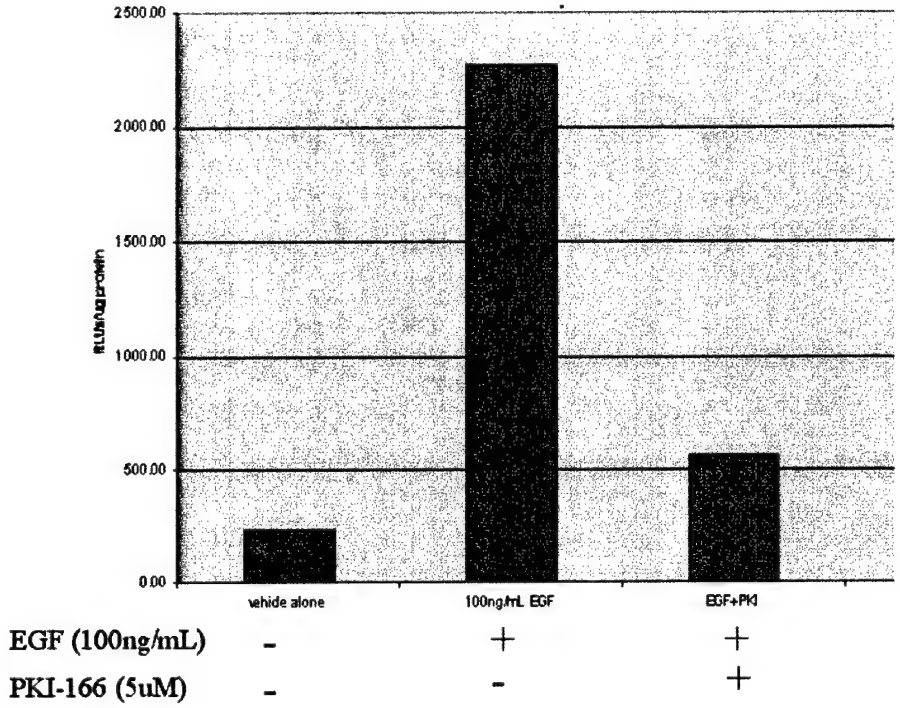

Figure 8. Effect of PKI on EGF Stimulation of MAPK in LAPC9 Cell Suspensions. LAPC9 AI tumors were harvested from SCID animals and cell suspensions were generated. The suspensions were transfected in triplicate with TSTA-Elk and cells were treated with vehicle alone, EGF and EGF+PKI166. After 48 h cell extracts were prepared and luciferase activity was measured by luminometry. Activity is in RLU; relative luciferase units.

The results of Figure 8 show that EGF strongly stimulates TSTA-Elk activity in tumor suspensions and PKI166 inhibits the effect. The data argue that EGF can activate the MAPK pathway in AI cells and that the effect can be inhibited by PKI166.

The data suggested at this point that AI cells are capable of responding to EGF signaling but EGF may not be the pathway naturally driving MAPK activity in vivo. This is a complex idea that suggests that active MAPK and response to MAPK stimulants is a key aspect of the AD to AI transition but the natural inducer remains unknown.

To address this idea, we decided to treat AD cells with EGF and determine if it stimulated transition of AD cells to the AI state in Nude female mice. If we could force the transition to become dependent upon EGF perhaps we could observe an effect of the PKI166 inhibitor on MAPK signaling in vivo. We therefore transfected the TSTA-Elk

plasmid into LAPC9 AD tumor suspensions in the presence of EGF and PKI and implanted the cells into female nude mice.

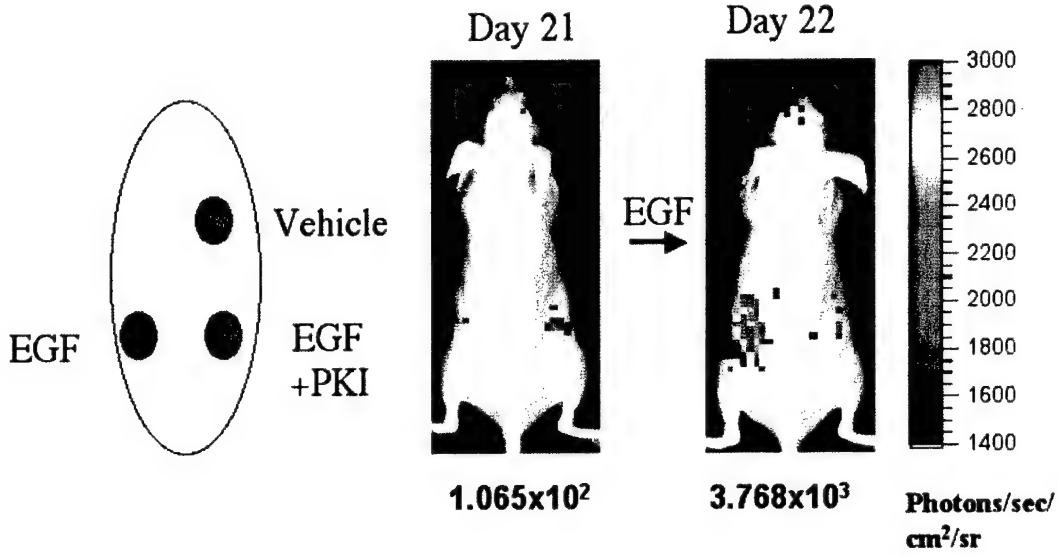

Figure 9. Effect of PKI on EGF-mediated MAPK Activity in LAPC9 AD cells. LAPC9 AD tumor cell suspensions were prepared and transfected with the TSTA-Elk plasmid. The cells were divided into three groups. One group was treated with vehicle, one with EGF and another with EGF+PKI. The cells were then implanted into three positions on the back of a female nude mice. After 21 days the mice were imaged to determine the baseline TSTA-Elk1 activity. The mice were then injected with 2.5 micrograms of EGF and imaged 24 hours later.

The data in Figure 9 show that EGF-treated AD cells do not possess a high basal level of MAPK activity on day 21 after implantation. However, when the mice are injected with EGF on Day 21, cells that had been previously treated with EGF in culture (see Map to left of Figure) displayed a marked increase (~37 fold) in MAPK activity (compare day 21 to day 22). However, cells that were treated with EGF+PKI166 in culture were not able to respond. Vehicle-treated cells were also unresponsive.

One interpretation of these data is that only a subpopulation of AD cells are initially responsive to EGF but this is not apparent in a large population. This subpopulation then grows out in the animal and retains the ability to respond to EGF. This idea would suggest that the EGF pathway per se is not driving natural AI cancer but a subpopulation of EGF-treated AD cells can respond to EGF and transition into AI. We note that of the three cell populations implanted into the backs of Nude mice, only the cells that were pre-treated in culture with EGF were able to develop into 0.5-cm AI tumors (not shown). Pre-treatment with PKI166 inhibited tumor growth stimulated by EGF. We also note that GAL4-Elk expression is dependent upon on AR so AR must be active in these EGF-stimulated AI tumors.

As mentioned earlier, we have an ongoing study to examine the ability of AD and AI cells to respond to EGF and PKI166 in culture and in vivo. The preliminary data suggest again that AI cells have high basal activity and respond immediately to EGF in culture. AD cells as a population do not respond to EGF in culture but as shown above

the EGF-treated AD cells do eventually gain the ability to respond as they transition to AI. PKI166 blocks this EGF-dependent transition.

The main conclusion is that the MAPK pathway is clearly functioning at a higher basal level in AI cells and somehow maintains the ability to respond robustly to EGF. However we find it unlikely that EGF is actually driving the tumor growth in the natural AI state because of the data in figures 7-9.

Task 5: Perform nuclear localization tests of AR (months 11-36)

One of the key questions regarding AR function during androgen independent prostate cancer is whether it has the ability to localize the nucleus in the presence of castrate levels of ligand. Figure 3 of Zhang et al. (2003) (appended) shows by immunohistochemistry that AR localizes to the nucleus of androgen dependent cells in tumors but appears to largely exit the nucleus upon castration of male SCID mice bearing the tumors. In contrast AR apparently re-enters the nucleus after the AD tumors transition to the AI state. Thus, AR re-enters the nucleus at castrate levels of DHT in live animals. Other experiments are in progress to determine if there is a link between the elevated basal levels of MAPK and the AR translocation to the nucleus.

Task 6: Perform chromatin immunoprecipitation on AD and AI tumors.

A central question in the prostate cancer field is whether AR binds to its responsive promoters in AI cancer and drives transcription. This idea has never been directly tested. In Zhang et al. (2003) we performed chromatin immunoprecipitation on LAPC9 AD and AI tumors to show that AR bound directly to the PSA enhancer in AD cells but fell off the enhancer upon castration. The decrease in binding correlated with a decrease in nuclear localization of AR. However, upon transition to the AI state the AR re-acquired the ability to bind to the enhancer. We found that transcription complexes did not dissociate completely during castration. RNA polymerase II (pol II) and its general factor TFIIB bound to the promoter even after castration. However, the bulk of pol II moved from an elongating position downstream of the promoter back to the promoter. We postulated that the transcription complex at a promoter remains in a poised state during castration to facilitate return to the active mode as cells transition to AI. This idea and related issues are discussed in the appended publications.

Task 7: Perform immobilized template assay.

We had hoped by this point to perform a biochemical analysis of the transcriptional machinery using an immobilized template assay but the in vivo analyses were pushed up and we have delayed implementation of the biochemistry. We are however planning on resuming this approach in the next year.

Key Research Accomplishments:

Accomplishments directly related to the TSTA system, which measures AR function

- Creation of the TSTA adenovirus
- Demonstration that the adenovirus-based TSTA system can measure androgen signaling in tumors in live animals.
- Demonstration that AR is fully active in AI cancer
- Demonstration that the TSTA system can detect the effect of anti-androgens like flutamide in tumors within live animals.

Accomplishments directly related to the TSTA-Elk System system, which measures AR and MAPK function

- Cloning of the TSTA-Elk plasmid.
- Demonstration that the TSTA-Elk system accurately measures MAPK signaling in cell culture.
- Demonstration that the TSTA-Elk system can detect the effect of MAPK pathway inhibitors like PKI166.
- Demonstration that TSTA-Elk responds to and measures EGF signaling in tumors in live animals.
- Demonstration that the TSTA-Elk system can detect the effect of the EGF pathway inhibitors like PKI166 in tumor growth assays.

Accomplishments directly related to AR function in AI cancers including nuclear localization and transcription complex assembly in tumors

- Demonstration that AR localizes to the nucleus in AD tumors, leaves the nucleus upon castration and re-enters the nucleus in AI tumors.
- Demonstration that AR binds the PSA enhancer in AD and AI cells.
- Demonstration that RNA polymerase II transcription complexes do not dissociate upon androgen withdrawal but remain poised to be re-activated upon the transition to AI cancer.

Reportable Outcomes:

Two publications have resulted from this work:

1. Zhang, L., Johnson, M., Le, K., Sato, M., Ilagan, R., Iyer, M., Gambhir, S., Wu, L. and Carey, M. Interrogating Androgen Receptor Function in Recurrent Prostate Cancer. Cancer Research 63: 4552-4560, 2003.

2. Sato, M., Johnson, M., Zhang, L., Zhang, B., Le, K. Gambhir, SS, Carey, M., Wu, L. Optimization of Adenoviral Vectors to Direct Highly Amplified Prostate-Specific Expression for Imaging and Gene Therapy. Molecular Therapy. (in press).

Two transcription based imaging systems have been funded by this work:

1. The adenovirus-based TSTA system described in Zhang et al. 2003. The TSTA adenovirus is available upon request as are the plasmids employed to create it.

2. The plasmid based TSTA-Elk system for imaging AR and MAPK function.

Conclusions:

One of the key issues in the prostate cancer field is whether AR is fully functioning in AI cancer and what aspects of AI cell metabolism permit function (refs. 6-8). Our hypothesis was that elevated MAPK is a key component of the transition from AD to AI cancer.

Our work with the adenovirus based TSTA imaging system demonstrated that AR was indeed fully functional in AI cancer. We also showed by immunohistochemistry and chromatin immunoprecipitation that AR was present in the nucleus in AI cancer and bound to promoter DNA. We further showed that the transition to AI cancer rendered the tumor refractory to inhibition by flutamide. This result firmly establishes that the tumor is probably not synthesizing androgen to compensate for castration since, if this idea was correct, the flutamide would still inhibit (i.e., unless it was being inactivated within the tumor). Our data suggest that the cells are truly employing an androgen-independent pathway to promote cell growth even while AR is still active. This is in contrast to ideas where the AR is utilizing castrate levels of ligand to function.

One idea is that elevated MAPK is directly influencing AR function in the absence of ligand. This idea has emerged from numerous studies (reviewed in refs. 6-8) and elevated MAPK directly stimulates AR function in cell culture (ref. 10). Our goal was to develop a non-invasive imaging system to test this idea in a natural tumor environment as cells progressed into the AI state. The TSTA-Elk system was designed to read out MAPK activity only when AR was active. We showed in cultured cells that the system functioned properly. Our preliminary data in tumor suspensions and in tumors in live animals suggest that AI cells do indeed possess higher MAPK levels than AD cells. These animals have been shown to reproduce the clinical transition of humans cancers from the AD to AI state. Furthermore, AI cells are primed to respond to MAPK inducers like EGF and can employ EGF to drive cell proliferation. However, AI cells can grow in the absence of elevated levels of EGF and therefore we suspect that another MAPK inducer is driving activity in the natural AI state. This idea was reinforced by the inability of PKI166 to function on natural AI tumors but it did have an effect when the AD-AI transition was facilitated by EGF.

Our immediate efforts will focus on completing the characterization and implementation of the TSTA-Elk system for imaging during tumor progression. Two issues will dominate our future efforts: 1. How MAPK is influencing AR function? 2. What is driving MAPK activity in the tumor?

The implications of our study are the following. First, we have developed a non-invasive imaging system to measure specific pathways related to prostate cancer progression. The systems may ultimately have clinical utility but await successful protocols for introducing such vectors into humans and must be transitioned from an optical method (CCD) to more clinically relevant imaging schemes like positron emission tomography (PET). Second, we are homing in on the mechanism of AR function in AI cancer and have developed both non-invasive imaging assays that can be coupled with cell based assays and

biochemical analysis of tumors to understand the changes in the AR transcriptional machinery that affect its function.

Terms Used:

AR: Androgen receptor (androgen dependent transcription factor that turns on prostate genes in vivo in response to dihyrotestosterone; DHT).
AD: Androgen dependent (refers to cancers that grow in male mice in the presence of physiological amounts of DHT).
AI: Androgen independent (refers to cancers that grow in castrated males or female mice).
CCD: Charge coupled device (an optical imaging system that can detect light generated by the luciferase-D-Luciferin reaction in live animals).
EGF: Epidermal growth factor (the ligand that activates the EGF receptor, a tyrosine kinase that activates the MAPK pathway).
ERK1/2: Extracellular response kinases (specific MAPKs involved in cell proliferation).
GAL4-VP16: A fusion of the yeast GAL4 DNA binding domain to the Herpes Simplex Virus VP16 transcriptional activation domain (a chimeric transcriptional activator with a unique specificity and potency not found in mammalian cells; used to amplify the AR signal to generate sufficient luciferase to visualize by CCD-based optical imaging).
GAL4-Elk1: A fusion of the GAL4 DNA binding domain to the MAPK inducible transcription factor Elk-1 (used to detect MAPK signals indirectly via a transcriptional output; much more sensitive and non-invasive method for visualizing MAPK activity in tumors within a living animal).
MAPK: mitogen activated protein kinase (phosphorylates Elk-1 and other proteins necessary for cell proliferation).
PKI166: A drug that inhibits EGF receptor tyrosine kinase.
TSTA: Two step transcriptional activation (measures AR function and refers to an transcription-based optical imaging system).
TSTA-Elk: Two step transcriptional activation system replacing GAL4-VP16 with GAL4-Elk1 (measures AR and MAPK function).
LAPC9: Los Angeles Prostate Cancer 9 (one of many LAPC mouse models of cancer: a SCID mouse bearing a human prostate cancer).

References:

1. Adams, J. Y., M. Johnson, M. Sato, F. Berger, S. S. Gambhir, M. Carey, M. L. Iruela-Arispe, and Wu, L. 2002. Visualization of advanced human prostate cancer lesions in living mice by a targeted gene transfer vector and optical imaging Nat. Med. **8:**891-7.

2. Iyer, M, Wu, L., Carey, M., Wang, Y., Smallwood, A. and Gambhir, S. S. 2001. Two-step Transcriptional Amplification as a Method for Imaging Reporter Gene Expression Using Weak Promoters. Proc. Natl. Acad. Sci. (USA) **98,** 14595-600.

3. Zhang, L., Adams, J., Billick, E., Ilagan, R., Iyer, M., Le, K., Smallwood, A., Gambhir, S., Carey, M. and Wu, L. 2002 Molecular Engineering of a Two-step Transcription Amplification (TSTA) System for Transgene Delivery in Prostate Cancer. Mol. Ther. **5:**223-3. 2002

4. Zhang, L., Johnson, M., Le, K., Sato, M., Ilagan, R., Iyer, M., Gambhir, S., Wu, L. and Carey, M. 2003. Interrogating Androgen Receptor Function in Recurrent Prostate Cancer. Cancer Res. **63:**4552-4560.

5. Sato, M., Johnson, M., Zhang, L., Zhang, B., Le, K. Gambhir, SS, Carey, M., Wu, L. Optimization of Adenoviral Vectors to Direct Highly Amplified Prostate-Specific Expression for Imaging and Gene Therapy. Mol. Ther. (in press).

6. Abate-Shen, C., and Shen, M.M. 2000. Molecular genetics of prostate cancer Genes Dev. **14:**2410-34.

7. Gelmann, E. P. 2002. Molecular biology of the androgen receptor J Clin Oncol. **20:**3001-15.

8. Feldman, B. J., and Feldman D. 2001. The development of androgen-independent prostate cancer Nat Rev Cancer. **1:**34-45.

9. Mellinghoff, I. K., C. Tran, and C. L. Sawyers 2002. Growth Inhibitory Effects of the Dual ErbB1/ErbB2 Tyrosine Kinase Inhibitor PKI-166 on Human Prostate Cancer Xenografts. Cancer Res. **62:**5254-9.

10. Abreu-Martin, M. T., A. Chari, A. A. Palladino, N. A. Craft, and C. L. Sawyers 1999. Mitogen-activated protein kinase kinase kinase 1 activates androgen receptor-dependent transcription and apoptosis in prostate cancer Mol. Cell. Biol. **19:**5143-54.

Appendices:

Item 1. **Zhang, L., Johnson, M., Le, K., Sato, M., Ilagan, R., Iyer, M., Gambhir, S., Wu, L. and Carey, M.** Interrogating Androgen Receptor Function in Recurrent Prostate Cancer. Cancer Research 63: 4552-4560, 2003.

Item 2. **Sato, M., Johnson, M., Zhang, L., Zhang, B., Le, K. Gambhir, SS, Carey, M., Wu, L.** Optimization of Adenoviral Vectors to Direct Highly Amplified Prostate-Specific Expression for Imaging and Gene Therapy. Molecular Therapy. (in press).

[CANCER RESEARCH 63, 4552–4560, August 1, 2003]

Interrogating Androgen Receptor Function in Recurrent Prostate Cancer[1,2]

Liqun Zhang, Mai Johnson, Kim H. Le, Makoto Sato, Romyla Ilagan, Meera Iyer, Sanjiv S. Gambhir, Lily Wu, and Michael Carey[3]

Departments of Biological Chemistry [L. Z., K. H. L., R. I., M. C.] and Urology [M. J., M. S., L. W.], Crump Institute of Molecular Imaging [S. S. G., L. W., M. C.], and Department of Molecular and Medical Pharmacology [M. I., S. S. G.], University of California, Los Angeles, School of Medicine, Los Angeles, California 90095

ABSTRACT

The early androgen-dependent (AD) phase of prostate cancer is dependent on the androgen receptor (AR). However, it is unclear whether AR is fully functional in recurrent prostate cancer after androgen withdrawal. To address this issue we interrogated AR signaling in AD and recurrent prostate cancer xenografts using molecular imaging, chromatin immunoprecipitation, and immunohistochemistry. In the imaging experiments, an adenovirus bearing a two-step transcriptional activation cassette, which amplifies AR-dependent firefly luciferase reporter gene activity, was injected into tumors implanted into severe combined immunodeficiency mice. A charge-coupled device optical imaging system detected the initial loss and then resumption of AR transcriptional activity in D-luciferin-injected mice as tumors transitioned from AD to recurrent growth. The results of chromatin immunoprecipitation and immunohistochemical localization experiments correlated with the Ad two-step transcriptional activation imaging signal. AR localized to the nucleus and bound to the endogenous prostate-specific antigen enhancer in AD tumors but exited the nucleus and dissociated from the enhancer upon castration. However, AR reentered the nucleus and rebound the prostate-specific antigen enhancer as the cancer transitioned into the recurrent phase. Surprisingly, RNA polymerase II and the general factor TFIIB remained bound to the gene throughout the transition. Our data support the concept that AR is fully functional in recurrent cancer and suggest a model by which a poised but largely inactive transcription complex facilitates reactivation by AR at castrate levels of ligand.

INTRODUCTION

Prostate cancer growth is controlled by AR[4] (1), a member of the steroid receptor subfamily of nuclear receptors (2). In the presence of its ligand DHT the bulk of AR moves from the cytoplasm to the nucleus (3, 4), binds to 15-bp DNA elements (AREs) in enhancers and promoters, and activates expression of genes involved in prostate metabolism including PSA.

PSA is a secreted kallikrein protease widely used for evaluating treatment and progression of cancer, although it has some drawbacks in prognostic utility (5). The PSA promoter and enhancer have been delineated and contain AREs necessary for transcriptional activity in AD cancer cell lines such as LNCaP (6–12). A 440-bp core segment of the enhancer plays the major role in androgen responsiveness (10). Multiple dimers of AR bind cooperatively to a cluster of AREs in the core enhancer, and synergistically activate transcription (13, 14) via interaction with coactivators that recruit pol II and its associated factors (1). DHT-dependent binding of AR to the PSA enhancer has been studied extensively in AD LNCaP cells using ChIP but has not yet been evaluated in AD or recurrent tumors (15–17).

A central role for AR in AD prostate cancer has been inferred from the observation that tumor growth initially ceases with treatments that lower the concentration or effectiveness of DHT. Although secreted PSA levels decrease as AR activity is diminished (18), the cancer eventually transitions from the AD state to a recurrent or AI state upon failure of androgen withdrawal therapies (19–21). As the cancer transitions, the levels of secreted PSA rise again, implying that AR is functional.

In many recurrent cancers the AR gene is amplified and/or AR is overexpressed (22, 23). The relevance of AR overexpression in cancer is supported by transgenic animal studies, where forced overexpression of murine AR from the probasin promoter leads to development of high-grade prostatic intraepithelial neoplasia, a precursor to prostate cancer (24). It has been hypothesized that in recurrent cancer, overexpressed AR can function by using castrate levels of DHT or adrenal androgens (22, 25).

Mutations in AR are occasionally associated with recurrent cancer. Certain mutations in the ligand-binding domain of AR permit it to function with alternative ligands in cell culture and *in vivo* (21). Additionally, somatic mutations identified in the transgenic adenocarcinoma of mouse prostate model revealed a correlation between reduced androgen dependence and the presence of mutations in AR functional domains known to interact with coactivators (26). In summary, it is plausible that mutation of AR facilitates interactions with coactivators in the absence of ligand or the presence of alternative ligands.

MAPK has also been postulated to augment AR activity in the absence of ligand (19–21, 27–29). Elevated MAPK levels have been observed in advanced prostate cancer specimens from patients and in recurrent xenograft models (30, 31). Several receptor tyrosine kinases or growth factors that signal through MAPKs activate AR-responsive reporter genes in an AI manner when overexpressed in cell culture (19–21, 27–29). A receptor tyrosine kinase inhibitor that targets the epidermal growth factor receptor pathway inhibits AR activity and tumor growth in animal models (31).

Additional support for a direct role of AR in recurrent cancer growth comes from cell culture studies. Lowering AR levels in an AI LNCaP cell line by injection of an AR-targeted hammerhead ribozyme or AR antibodies reduces cell proliferation (32). It has been suggested that AR may function not by binding DNA but through cytoplasmic interaction with signaling molecules that activate the MAPK pathway (33, 34). However, the effect of AR on PSA gene transcription in at least one AI cell line probably involves DNA

Received 3/13/03; accepted 5/27/03.

The costs of publication of this article were defrayed in part by the payment of page charges. This article must therefore be hereby marked *advertisement* in accordance with 18 U.S.C. Section 1734 solely to indicate this fact.

[1] Supported by Department of Defense Grant PC020177 (to M. C.), CaPCURE Grant (to M. C. and S. S. G.), Department of Defense CDMRP PC000046 (to L. W.), Department of Defense PC991019 (to Charles Sawyers, UCLA School of Medicine, and M. C.), an interdisciplinary seed grant from the Jonsson Comprehensive Cancer Center (to M. C., L. W., and S. S. G.), R01 CA82214 (to S. S. G.), SAIRP R24 CA92865 (to S. S. G.), and Department of Energy Contract DE-FC03-87ER60615 (to S. S. G.). L. Z. is supported by United States Department of Health and Human Services Institutional National Research Service Award #T32CA09056. R. I. is supported by a Research Training in Pharmacological Sciences Award #T32JM08652.

[2] Supplementary data for this article are available at *Cancer Research Online* (http://cancerres.aacrjournals.org).

[3] To whom requests for reprints should be addressed, at Department of Biological Chemistry, University of California Los Angeles School of Medicine, Los Angeles, CA 90095-1737. Phone: (310) 206-7859; Fax: (310) 206-9598; E-mail: mcarey@mednet.ucla.edu.

[4] The abbreviations used are: AR, androgen receptor; ARE, androgen response element; AD, androgen-dependent; ADc, androgen-dependent castrated; AI, androgen-independent; CCD, charge coupled device; CHIP, chromatin immunoprecipitation; DHT, dihydroxytestosterone; LAPC, Los Angeles prostate cancer; MAPK, mitogen-activated protein kinase; pol II, RNA polymerase II; PSA, prostate-specific antigen; SCID, severe combined immunodeficiency; TSTA, two-step transcriptional activation; pfu, plaque-forming unit(s); CMV, cytomegalovirus; Ad, adenovirus; MOI, multiplicity of infection.

binding, because the PSA enhancer requires some of its natural AREs for activity, although other transcription factors also contribute (35).

Despite these intriguing cell culture studies, direct measures of AR activity and binding of AR to responsive genes have not been demonstrated in recurrent tumors. This is an important issue for developing pharmaceuticals targeted to recurrent cancer, the most deadly form of the disease in men. The goal of our study was to confirm AR function in the context of human xenograft tumors implanted into SCID mice. We used the LAPC9 model, a human prostate cancer derived from a bone metastasis (36). LAPC9 tumors express PSA and wild-type AR, and on castration of the SCID mice, the tumor transiently halts growth and gradually transitions into the recurrent state. Continued passage of the tumor in castrated mice generates a stable AI model, which expresses AR and PSA.

We used four tools to study AR function in the LAPC9 tumors: secreted PSA levels, immunohistochemistry, ChIP, and molecular imaging. The PSA levels permitted us to confirm that the tumor responded to androgen deprivation in castrated animals and rose during transition to recurrent cancer. Immunohistochemistry allowed us to monitor nuclear localization, an important parameter of AR function. ChIP enabled us to directly monitor specific AR binding to the endogenous PSA gene within tumors. Gene expression-based molecular imaging is a new technology that permitted us to noninvasively visualize transcriptional activity during cancer progression (37–40).

The molecular imaging technology uses a cooled CCD camera, which detects light emitted from living animals when a firefly luciferase reporter gene is expressed in the presence of its substrate D-luciferin (41). The short half-life of luciferase in combination with highly active reporter genes facilitates dynamic measurements of expression occurring over weeks within tumors implanted into an animal (42). Our imaging system is based on the PSA regulatory region because of its AR responsiveness and prostate specificity (9).

In a previous study, we duplicated the core PSA enhancer and significantly augmented AR-responsive firefly luciferase activity in cell culture (43). An adenovector bearing this imaging cassette, AdPBC, detected distal metastatic lesions in xenograft models using the CCD optical imaging system (44). The overall activity of the AdPBC reporter cassette was only 5% that of AdCMV-luciferase, the benchmark for CCD imaging studies, making it difficult to dynamically monitor the androgen response. To additionally improve the signal we used the TSTA strategy. The duplicated PSA regulatory region was linked to the gene for the potent transcription activator GAL4-VP16. When GAL4-VP16 is synthesized it acts on a GAL4-responsive firefly luciferase reporter gene resulting in amplified levels of expression (45). We previously optimized the system by varying the numbers of GAL4 sites and VP16 activation domains (46).

In this paper we incorporated the optimal TSTA system into a replication-deficient adenovirus (47) to create AdTSTA. Adenovirus exhibits a high infection efficiency and is widely used in gene transfer studies in animals and humans (48). We injected AdTSTA into LAPC9 AD and recurrent tumors implanted into the flanks of SCID mice, and imaged the activation, inactivation, and reactivation of AR activity during cancer progression. Immunohistochemical staining and ChIP of AR on the PSA regulatory region in the various stages of cancer growth supported the concept that AR is fully active in recurrent cancer. ChIP data also suggested a model whereby the RNA pol II transcription complexes on AR-responsive genes do not disappear in the absence of androgen but remain poised to resume activity.

MATERIALS AND METHODS

Adenovirus Constructs. AdTSTA was generated from the optimal TSTA plasmid (46). A second *Not*I site 5′ from the PBC enhancer was removed to create unique *Not*I site in the vector. A *Sal*I-*Not*I fragment containing the core BCVP2G5-Luc fragment was excised by *Not*I and partial *Sal*I digestion, and inserted into the *Sal*I-*Not*I site of pShuttle (Q-Biogene, Carlsbad, CA), which was then incorporated into the adenovirus vector AdEasy through homologous recombination. AdCMV was generated as described previously (44). The viruses were packaged and propagated in 293A cells. The virus was scaled up, purified via a CsCl gradient, and titered by plaque assays on 293 monolayers (infectious units = plaque-forming units). Virus was stored at $\sim 10^{11}$ pfu/ml in 10 mM Tris-HCl, 1 mM $MgCl_2$, and 10% glycerol. TSTA plasmid vectors that contain convenient restriction sites for removing PBC and replacing it with any promoter have been constructed and will be provided on request.

Cell Culture and Xenografts. The human prostate cancer cell line LNCaP was grown in RPMI 1640 supplemented with 10% fetal bovine serum and 1% penicillin/streptomycin solution. HeLa, MCF-7, and HepG cells were cultured in DMEM with 10% fetal bovine serum and 1% penicillin/streptomycin. Before transfection, cells were transferred for 24 h into medium containing 5% charcoal-stripped serum (Omega Sci., Tarzana, CA). The synthetic androgen methylenetrienolone (R1881; NEN Life Science Products, Boston, MA) was added to "ligand-positive" samples where indicated.

Human prostate tumor xenografts were generated on SCID mice as described previously (36). Briefly, $\sim 1 \times 10^6$ LAPC-9 tumor cells generously provided by Dr. Charles Sawyers (UCLA School of Medicine, Los Angeles, CA) were mixed 1:1 with Matrigel (BD Scientific) and implanted s.c. on the left flank of male SCID (C.B. −17 *Scid/Scid*) mice. The AI sublines were passaged several rounds in castrated male mice. Single-cell suspension cultures were maintained on Pre-BM/GM medium (Clonetics, Walkersville, MD). Alternatively, tumors were extracted from founder mice, minced into ~0.2-mm cubes, bathed in Matrigel, and implanted s.c. onto the left flanks of SCID mice.

Virus Activity Assays. For firefly luciferase assays, the cultured cells were infected with AdTSTA or AdCMV at a MOI of 0.1. After 48 h, the cells were harvested and lysed using the passive lysis buffer provided in the firefly luciferase assay kit (Dual-Reporter Luciferase Assay System; Promega, Madison, WI). Firefly luciferase activities of 5% of the cell lysates supplemented with 100 μl of D-luciferin were measured using a luminometer (Lumat 9507; (Berthold Technologies, Oak Ridge, TN) with an integration time of 10 s.

Immunoblot Analysis of GAL4-VP16 Expression. LNCaP cells were grown in 10-cm dishes and infected with AdTSTA at MOI 10. Forty-eight h later the cells were harvested and lysed with radioimmunoprecipitation assay buffer (10 mM Tris-HCl, 150 mM NaCl, 0.1% SDS, 1% DOC, 1 mM EDTA, and 1% NP40). Protein concentrations of the extracts were normalized (Bio-Rad Dc protein assay kit), and the samples were fractionated on 4–15% gradient acrylamide gels (Bio-Rad, Hercules, CA) and subjected to immunoblot analysis with rabbit polyclonal antibodies generated against intact GAL4-VP16 or loading control proteins.

CCD Imaging of Firefly Luciferase Expression. For the naïve mice, 10^7 pfu of AdTSTA or AdCMV suspended in 100 μl PBS was injected via the tail vein. For the LAPC9 xenografts, a total of 10^7 pfu of AdTSTA or AdCMV in 40 μl PBS was injected directly into the 0.5-cm diameter tumor xenografts at multiple locations. To ensure adequate distribution throughout the tumor, the injection was carried out twice on 2 sequential days. The virus was allowed to express the encoded genes and distribute throughout the tissue for 3–4 days before imaging. At the days specified in the figures, the mice were anesthetized and injected with ~150 mg/kg D-luciferin (~3 mg/mouse). Light signals (CCD images) were obtained using a cooled IVIS CCD camera (Xenogen, Alameda, CA), and images were analyzed with IGOR-PRO Living Image Software, which generates a pseudoimage with an adjustable color scale. We determined the maximum photons/second of acquisition/cm^2 pixel/steridian within a region of interest to be the most consistent measure for comparative analysis. The imaging results correlated closely with luminometry of tissue extracts. Typically our acquisition times ranged from 1 to 10 s.

Tumor Immunohistochemical Analysis. Immunohistochemistry was performed on paraffin-embedded tumor sections with antigen retrieval. Tissue sections were incubated at 4°C overnight with anti-AR 5 μg/ml (UpState, Charlottesville, VA). After stringent blocking, washing, and incubation with

multilink (BioGenex, San Ramon, CA), and alkaline phosphatase label for 20 min at room temperature, sections were washed and developed according to the manufacturer's instructions (BioGenex).

Secreted PSA and Serum DHT Measurements. Blood was withdrawn from the mice by retro-orbital bleeding, and plasma was collected. PSA levels were measured using a PSA ELISA kit (American Qualex, San Clemente, CA), whereas the DHT levels were measured using a DHT ELISA kit (Alpha Diagnostic International. San Antonio, TX). All of the measurements were performed in triplicate.

Tumor Chromatin Immunoprecipitation. Tumors were extracted from the mice and washed with ice-cold PBS. The tumors were quickly minced and immersed in 1% formaldehyde solution, where they were additionally minced and homogenized using a glass dounce. The total incubation in formaldehyde solution was for 30 min. Before sonication, the cell suspensions were washed for 10 min each in solution I containing 0.25% Triton, 10 mM EDTA, 1 mM EGTA, and 10 mM HEPES (pH 7.5), and in solution II containing 0.2 M NaCl, 1 mM EDTA, 1 mM EGTA, and 10 mM HEPES (pH 7.5). Extracts were obtained by 8 × 15 s sonication in lysis buffer containing 1% SDS and 10 mM EDTA using a Fisher Scientific Model 550 sonicator at setting 4 with a microtip. Chromatin was purified from insoluble debris by microcentrifugation at 15,000 rpm for 20 min.

To perform immunoprecipitation, the chromatin was diluted 1:7 in dilution buffer containing 70 mM HEPES (pH 7.5), 2.5 mM NaCl, 1.5 mM EDTA, 1.5% Triton, and 0.6% deoxycholate. The extracts were precleared with preimmune IgG together with Sepharose A or G agarose beads (Amersham, Piscataway, NJ) for 1 h at 4°C. Precleared extracts were incubated with 4–6 μg of specific antibodies at 4°C overnight followed by incubation with 30 μl of agarose A or G beads for 1 h the next day. The antibodies included the N20 and C19 AR antibodies from Santa Cruz Biotech, the pol II CTD8WG16 monoclonal from QED Bioscience (San Diego, CA), and a TFIIB antibody generated in our laboratory. The beads were washed twice with buffer containing 50 mM HEPES (pH 7.5), 0.15 M NaCl, 1 mM EDTA, 1% Triton, 0.5% deoxycholate and 0.15% SDS followed by wash with LNDET buffer containing 0.25 M LiCl, 1% NP40, 1% sodium deoxycholate, 1 mM EDTA, and 10 mM Tris (pH 8.0). The protein-DNA complexes were then eluted from the beads with 30–50 μl elution buffer containing 1% SDS and 1 mM $NaHCO_3$. The eluates were diluted with 10 mM Tris (pH 8.0)-1 mM EDTA and incubated at 65°C overnight to reverse the cross-link. The samples were then treated with proteinase K at 100 ng/μl and RNAase A for 1 h at 55°C, and then extracted with phenol. The DNA was then precipitated with ethanol, resuspended in 30 μl water, and subjected to PCR analysis. Typically one 1-cm tumor yielded enough material for six PCR reactions. The input sample in the data shown in the ChIP experiments was typically 2% of the DNA added to a ChIP reaction.

The PCR analyses were performed with four sets of ^{32}P-labeled of primers: Enhancer: 5′ggtgaccagagcagtctaggtg3′ and 5′tgtttactgtcaaggacaatcgat3′; Promoter: 5′gtatgaagaatcggggatcgt3′ and 5′ gctcatggagacttcatctag3′; Middle: 5′tatgcttggggacaccggat3′ and 5′ttagagctggagtggaaggatat3′; Exon 5: 5′taatggtgtgcttcaaggtatcacg3′ and 5′gtgtccttgatccacttccggtaat3′

The PCR cycling protocol was 40 s at 94°C, 3 min at 75°C, 2 min at 65°C, followed by 20 cycles of 40 s at 94°C, 1 min at 65°C, and 2 min at 72°C, followed by a 10-min extension at 72°C. The PCR products were phenol-extracted, separated on 6% polyacrylamide gels, and autoradiographed by exposure to XAR-5 film.

RESULTS

AdTSTA Is AR-responsive in Cell-based Assays. The transcriptional activity of AR is the most relevant measure of its function *in vivo*. Our previous study used a plasmid expressing the TSTA system to study AR-mediated gene expression in cell culture (46). To monitor AR in live animal models of prostate cancer it was necessary to insert the TSTA cassette (Fig. 1*A*) into an adenovirus, which could be injected directly into tumors. The cassette was inserted into the

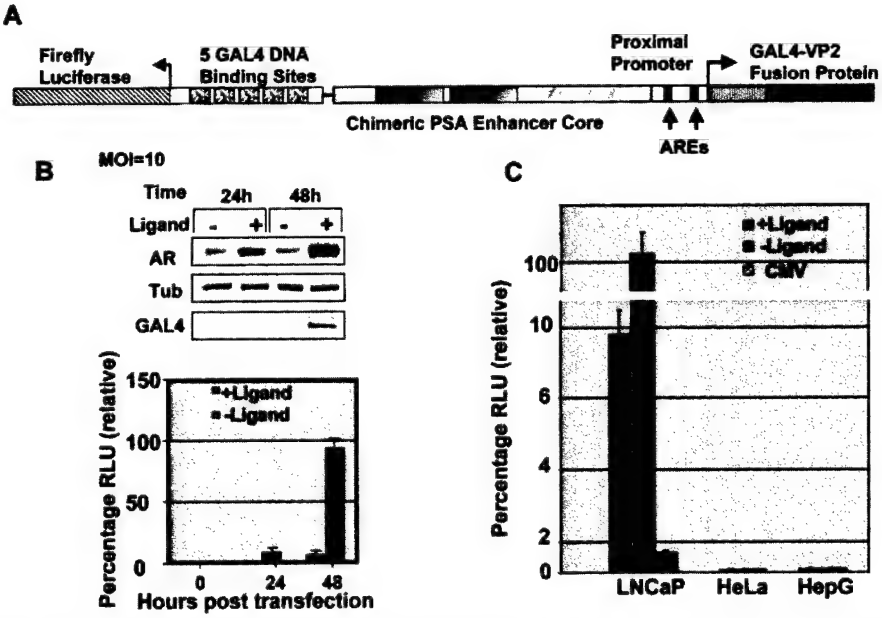

Fig. 1. Validation of the molecular imaging system in cell culture. *A*, a schematic of the AdTSTA imaging system. The *top portion* of the diagram shows the TSTA imaging cassette. The PSA enhancer from −4326 to −3935 was duplicated (the chimeric enhancer core) within the upstream regulatory region from −5322 to −3744 and attached to the proximal promoter from −541 to 1. Each enhancer bears a cluster of six AREs, and the promoter contains two AREs. The PSA regulatory region is shown expressing GAL4-VP2 bearing two NH_2-terminal herpes simplex virus 1 VP16 activation domains (amino acids 413–454) fused to the GAL4 DNA binding domain (amino acids 1–147). A GAL4-responsive promoter is fused in the divergent orientation to the PSA regulatory region. The GAL4-responsive promoter contains five 17-bp GAL4 sites upstream of the adenovirus E4 promoter driving firefly luciferase. The entire cassette was cloned into a shuttle vector and introduced into Ad5 deleted (△) for E1 and E3 using the AdEasy system. The virus was propagated in 293 cells, purified and titered. *B*, a demonstration of AdTSTA activity in cancer cell lines. LNCaP cells were infected with AdTSTA at a MOI of 10 for 1 h and treated with 10 nM R1881 (+*Ligand*) or vehicle (−*Ligand*). At the indicated time points, the cells were lysed with Reporter Lysis Buffer, and firefly luciferase activity was analyzed either by luminometry (*bottom panel*, *Y*-axis: Relative Luciferase Units/μg of total protein normalized to 100%) or by immunoblotting (*top panel*, *AR*, anti-AR; *Tub*, Anti-tubulin; GAL4, anti-GAL4-VP16). Samples were prepared in triplicate and the average reading is shown; *bars*, ±SE. The triplicate samples were mixed for immunoblot analysis. *C*,. LNCaP, HeLa, or HepG cells were infected with AdTSTA at a MOI of 0.1 for 1 h followed by treatment with 10 nM R1881. The cells were harvested 48 h later, and luciferase levels were measured. Data are normalized to the ligand-induced signal in LNCaP (100%). The AdCMV (MOI 0.1) signal in LNCaP is shown in ■ for comparison of the AdTSTA and AdCMV luciferase activity; *bars*, ±SE.

genome of adenovirus serotype 5 in which the E1 and E3 coding regions were deleted, which rendered the virus replication-deficient (47). The TSTA cassette comprises a modified PSA regulatory region containing two copies of the AR-responsive core PSA enhancer placed upstream of GAL4-VP2. GAL4-VP2 contains two copies of the VP16 activation domain fused to the GAL4 DNA binding domain. In the presence of androgen, GAL4-VP2 is synthesized and binds to five GAL4 binding sites positioned upstream of the adenovirus E4 core promoter, which drives high levels of firefly luciferase expression (Fig. 1). Luciferase was measured in cell culture by luminometry and *in vivo* in D-luciferin-injected live animals using a Xenogen cooled CCD optical imaging system (42).

To validate the androgen responsiveness of the TSTA system in the context of the adenoviral vector, we infected the model AD prostate cancer cell line, LNCaP, with AdTSTA (Fig. 1*B*). GAL4-VP2 and firefly luciferase levels were enhanced significantly in the presence of the synthetic androgen agonist R1881. The largest increase of luciferase activity was observed at the 48-h time point (Fig. 1*B*, *bottom*), which correlated with the appearance of GAL4-VP2 by immunoblot analysis (Fig. 1*B*, *top*).

The AdTSTA system maintained cell selectivity in culture (Fig. 1*C*). An example of these findings is shown for cells derived from prostate cancer (LNCaP), liver (HepG), and cervical cancer (HeLa). LNCaP is an AD prostate cancer cell line (49), which contains a mutant form of AR and secretes PSA (50, 51). AR expression is not observed in HeLa and HepG cells (data not shown). PCR analysis demonstrated that viral infectivity was similar within a 2-fold range among the cell lines tested (data not shown). The LNCaP cells displayed significantly higher firefly luciferase activity than HeLa and HepG, and responded to the androgen agonist R1881. MCF-7 cells (an AR-expressing breast cancer cell line), PC3 (an AR-negative prostate cancer cell line), and PC3 stably expressing AR were also tested. These lines displayed only a low basal level of TSTA expression and did not respond to R1881 (data not shown). Thus, the AdTSTA system responds to AR in AD prostate cancer cells. The residual signal present in LNCaP cells in the absence of ligand could be suppressed by addition of the AR antagonist casodex suggesting that the TSTA amplification system is sensitive enough to respond to trace androgen levels present in charcoal-stripped growth medium (data not shown).

The AdTSTA also achieved an activity level suitable for dynamic measurements in live animals. Side-by-side comparison in LNCaP cells demonstrated that AdTSTA displayed a ligand-induced firefly luciferase activity 10-fold greater than AdCMV (Fig. 1*C*) and nearly 200-fold greater than AdPBC (data not shown). The increased activity obtained by using the TSTA approach reduced the average CCD acquisition times from 5 min to a few seconds (*i.e., versus* AdPBC). The signal obtained from AdTSTA was tumor specific and robust. Direct intratumoral injection into LAPC9 AD xenografts demonstrated that AdTSTA was routinely twice as active as AdCMV. Additionally, AdTSTA, unlike AdCMV, did not generate a CCD signal in liver when injected via the tail vein into nontumor bearing SCID mice (Supplementary Fig. 2). The gain in signal obtained via the use of TSTA permitted us to perform direct measurements of AR function at various stages of cancer growth. The high level of activity also allowed us to reduce the viral dose from 10^9 pfu used in the AdPBC study to 10^7 pfu used here. The lower doses decrease the possibility of viral toxicity.

Molecular Imaging of AR Signaling in AD, ADc, and AI Tumors. To demonstrate the androgen responsiveness of the tumor model we first castrated male mice bearing LAPC9 AD tumors and measured serum PSA levels (Fig. 2). A decrease or plateau of serum PSA is indicative of successful hormone blockade therapy in humans.

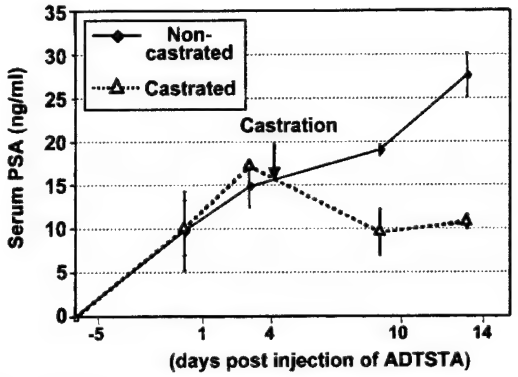

Fig. 2. Serum PSA measurements for AD and castrated mice. Serum ELISA measurements of PSA at various time points during tumor growth. Values are in ng/ml; *bars*, ±SE.

The xenograft data revealed that the PSA levels ceased rising and dropped slightly beginning 1 day after castration and remained flat, recapitulating the clinical response to androgen blockade therapy. At later time points, the PSA levels began to rise as tumors transitioned from AD to AI. Like PSA, the serum DHT levels decreased after castration to as low as 85% of the intact animals. However, DHT levels remained low even as PSA levels increased (data not shown).

Analysis of normal AD animals and animals castrated during tumor growth (ADc) revealed that the CCD imaging signal responded well to androgen withdrawal (Fig. 3*A*). The AdTSTA-injected AD tumors typically emitted $>10^7$ photons/sec/cm^2/sr on day 4 after virus injection. Castration on day 4 led to a >10-fold drop in the imaging signal by day 10 (Fig. 3*A graphs*; AD *versus* ADc; $P = 0.01$). In contrast, AdTSTA displayed robust activity in established AI tumors, and over the same time frame the signal increased. The increasing signal in AI *versus* AD tumors was intriguing, but we do not yet understand the cause. We have noted that AD tumors contain a large necrotic center, whereas AI tumors do not. It is plausible that the necrosis leads to some diminution in signal because of death of a subset of infected cells. Nevertheless, we can conclude from these data that the AR-responsive TSTA system is specifically responding to the loss of AR activity in the ADc tumor but that the activity is regained in established AI tumors.

Localization of AR in Tumors. The distribution of AR is sensitive to androgen depletion. AR is known to localize predominantly to the nucleus in the presence of androgen, whereas AR localization in the absence of androgen is diffuse, and distributes between the cytoplasm and nucleus (22). Immunohistochemical analyses of tumors from the sacrificed LAPC9 animals used in the imaging studies showed that AR was tightly localized to the nucleus of AD and established AI tumors (Fig. 3*B*). Typically 30–35% of the cells in the field stained strongly for nuclear AR, ~20% stained weakly, and the remainder displayed marginal or no staining in both AD and recurrent tumors. The staining in ADc was heterogeneous with a few cells showing nuclear staining but most showing a diffuse pattern of cytoplasmic staining.

The imaging and cytology data imply that AR initially ceases activity on castration probably because it exits the nucleus. However, AR resumes functioning in AI cancer. Several proposals have been made to explain how androgen-responsive genes could be activated in cells lacking physiological levels of androgen. In one model, other transcription factors like nuclear factor κB have been proposed to bind regulatory regions of androgen-responsive genes and partly substitute for AR in AI cancer (52). Nevertheless, the predominant nuclear location of AR in AI tumors implies that AR is functional. One

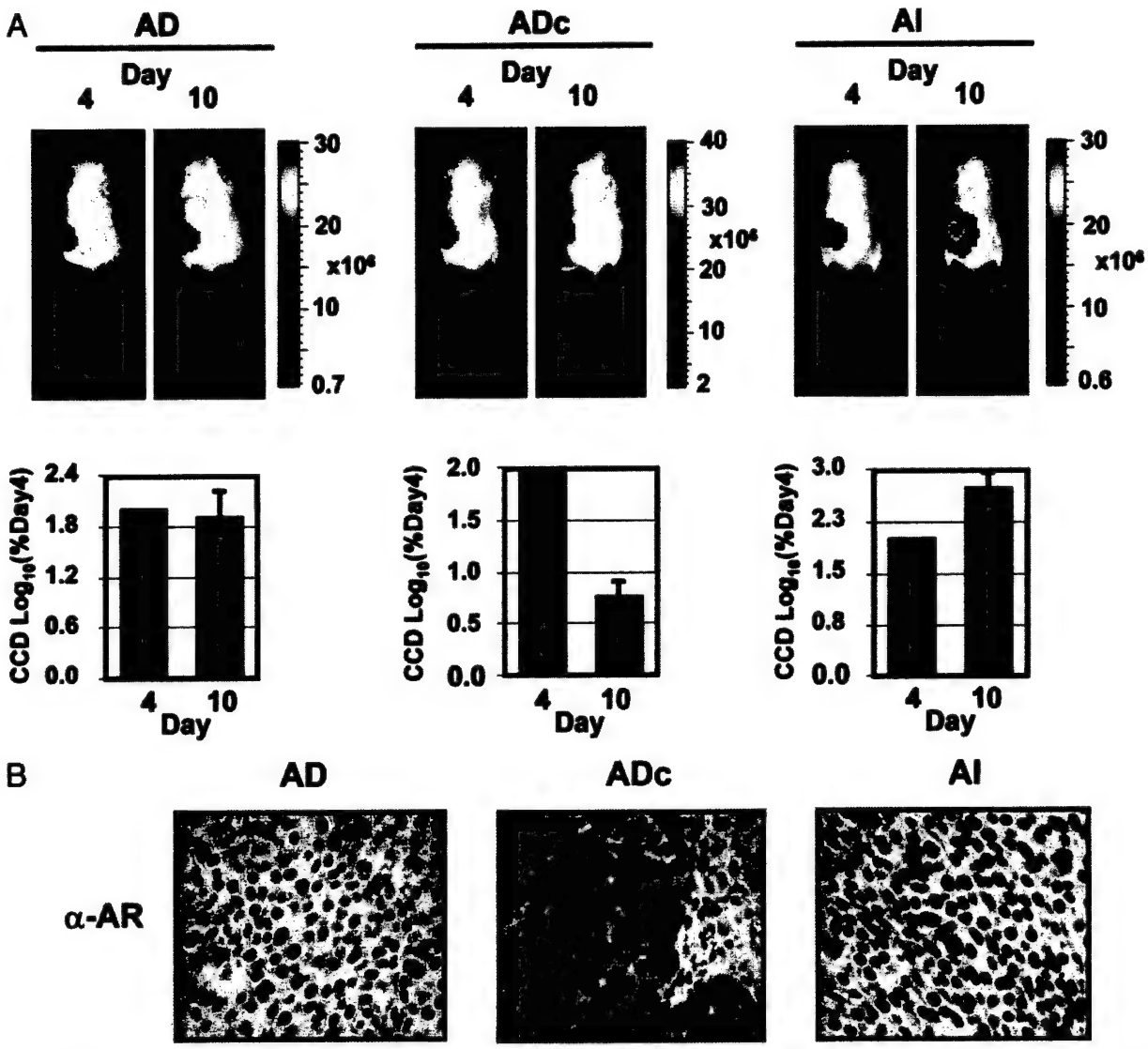

Fig. 3. Imaging AR signaling in LAPC 9 tumors. In *A*, SCID mice implanted with LAPC9 xenografts (>0.5 cm) were injected with 10^7 pfu of AdTSTA and the mice were imaged every 3–4 days until day 14. Representative mice at day 4 and day 10 after virus injection from the AD group, the castrated (on day 4) AD group (*ADc*), and the stable AI group. The *bar graph* summarizes a cohort of three or more and summarizes the log of the percentage change in signal from day 4 (*blue bars*) to day 10 (*purple bars*). Day 4 is set at 2 (*log 10*) in each case. The normalization to percentage change was necessary because there is variation in virus infectivity in different tumors. *B* shows representative immunohistochemical localization of AR in the AD, ADc, and AI tumors using anti-AR antibodies. AR stains *brown* against the blue-stained nuclei. For both AD and AI tumors, five high-power fields (×40) from multiple sample slides were counted, with an average of 100 cells/field. AR nuclear staining was recorded as percentage of cells counted. For AD tumors, cells with high AR nuclear staining are 33% (±5%), whereas cells with no or very faint AR nuclear staining is 19% (±6%) with the remainder staining at an intermediate intensity. For AI tumors, 30% (±2.7%) of the cells stained intensely, whereas cells with no or very faint AR nuclear staining was 22% (±3%). In conclusion, AR nuclear staining does not differ significantly between AD and AI tumors (P = 0.3 one tail and 0.7 two tail); *bars*, ±SE.

prediction of this hypothesis is that AR should bind directly to responsive enhancers and promoters in AI tumors.

Transcription Complex Assembly in Tumors. To determine whether AR was binding to the endogenous PSA regulatory region in AI tumors we used ChIP, which allows direct measurement of DNA binding to promoters and enhancers *in vivo* (Fig. 4). Previous ChIP experiments in AD LNCaP cells in culture have shown that AR and pol II bind to the PSA enhancer and promoter when the gene is active (15, 17). We analyzed AR binding to four regions of the gene in tumors: the enhancer, the promoter, an intervening region located between the enhancer and promoter, and downstream exon 5 (Fig. 4, *schematic*). Specific signals were confirmed by comparing the AR antibody signal to the background observed in a mock immunoprecipitation with IgG.

AR binding to both the PSA enhancer and promoter in the AD samples was detectable well above the IgG background (Fig. 4, *autoradiographs*). AR binding to the enhancer and promoter was specific because it was minimal within the middle intervening region and exon 5. Remarkably, AR bound nearly as well to the promoter and enhancer in the AI samples, demonstrating that it was fully functional in the presence of androgen withdrawal in a recurrent tumor.

The ChIP results were consistent when normalized to the signal from input DNA and averaged among three experiments. The binding of AR to the enhancer in AI tumors was typically only 20% lower than in AD tumors (Fig. 4, *graph*). In contrast, on ADc the binding of AR to the enhancer and promoter decreased 4-fold. There is still evidence of specific AR binding in ADc, because the signals on the enhancer and promoter are above the IgG background. The residual binding can

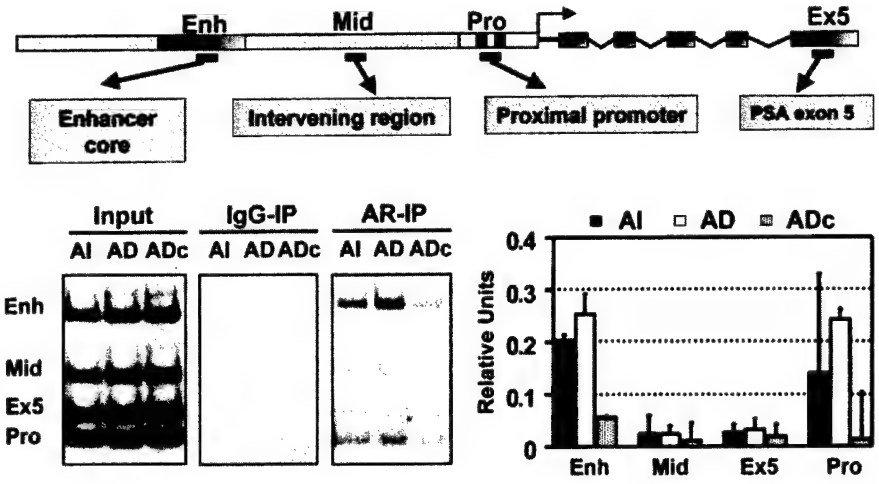

Fig. 4. Chromatin immunoprecipitation assays in LAPC9 tumors. The diagram in the *top panel* describes the PSA regulatory region. *Short black line underneath* indicates the positions targeted by PCR. *Enh*, enhancer core; *Mid*, intervening region; *Pro*, proximal promoter; *Ex5*, PSA exon 5 (for sequence coordinates see "Materials and Methods"). Tumors were isolated from mice sacrificed at day 10 (6 days after castration for ADc), minced, cross-linked with formaldehyde, and immunoprecipitated with anti-AR or a IgG (mock). Autoradiographs of the multiplex PCR reactions are shown for AD, AI, and ADc tumors. Input represents 2% of the DNA added to the immunoprecipitation reaction. Graph of multiple tumor ChIP analyses. The band intensities were analyzed using ImageQuant. Background values from a mock (IgG) ChIP were subtracted from each band and normalized to the signal from input DNA. *Bars*, ±SD of three values obtained in independent experiments.

be explained in part by the cytology data in which some AR remains in the nucleus even in ADc. Additionally, the PSA levels and imaging signals do not decrease to baseline in ADc but drop transiently as the tumor begins to transition to AI. This suggests that a small amount of residual AR-dependent PSA gene transcription occurs in the presence of castrate levels of ligand.

We initiated a mechanistic study to examine how transcription complexes respond to the presence and absence of hormone. We began by analyzing pol II, which should be found in both promoter-bound and elongating positions when the PSA gene is transcriptionally active (Fig. 5). Elongating pol II was measured by its binding to exon 5, which is easily discriminated from its binding to the promoter. As predicted, pol II binding was observed at both the promoter and downstream exon 5 in the AD and AI tumors. However, the ratio of the signal at exon 5 *versus* the proximal promoter shows that in AD and AI tumors pol II is primarily localized at exon 5.

Remarkably, in ADc tumors after castration, pol II remained bound to the gene at levels similar to those seen in AD tumors. However, pol II was positioned primarily at the promoter instead of exon 5 (Fig. 5, *top*, compare ratio of exon 5 to promoter). The overall amounts of the general factor TFIIB present at the PSA promoter also did not change in AD, ADc, and AI. Our interpretation of these findings is that the transcription complex remains intact after androgen deprivation, but a greater fraction of pol II is not actively transcribing in ADc *versus* AD and AI. A scatter plot summarizing four representative experiments is shown in Supplementary Data Fig. 2.

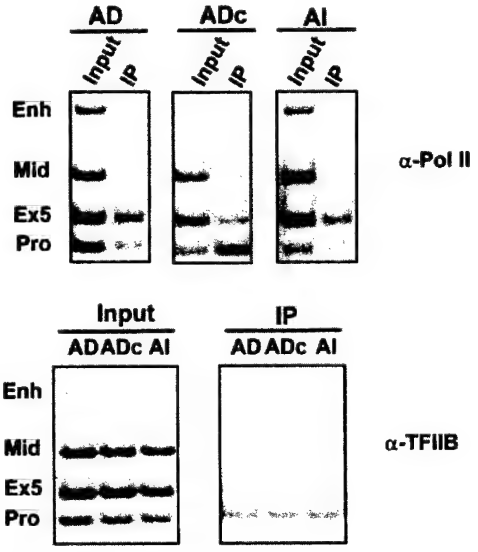

Fig. 5. ChIP analysis of RNA polymerase II and TFIIB from LAPC9 tumors. The bands are described in the Fig. 6 legend. Representative experiments from AD, AI, and ADc tumors are shown. The *top panels* are pol II, and the *bottom panels* are TFIIB.

Visualizing the AD-AI Transition. The original goal in developing the TSTA system was to monitor the loss and gain of AR-mediated transcription over time in a single individual as a tumor transitioned from ADc to AI. In a human, the failure of androgen deprivation therapy occurs gradually over a period of time that can vary from weeks to years. The LAPC9 models were originally adapted to an androgen-rich environment in immunodeficient male mice and then trained to grow in an AI manner in castrate or female mice, a process that can take months. However, we have found that the transition from AD to recurrent growth occurs rapidly as the tumor grows larger. In some animals the transition occurs quickly enough to monitor it over a short period of time as opposed to studying established AI tumors. The data in Fig. 6 illustrate a typical example of an animal undergoing the transition.

In this animal, we injected the AdTSTA virus, imaged 4 days later, and then castrated the animal when the tumor reached 1 cm. We observed that the PSA levels initially dropped up to 2.4-fold by day 10, 6 days postcastration, and then began rising again up to day 17. Over this same time frame, the imaging signal was high on day 4, reached a minimum by day 10, and then gradually rose again by day 17 (Fig. 6, *top*).

ChIP and immunohistochemical analyses on the tumor from the sacrificed animal revealed that AR resumed its nuclear localization and was bound primarily to the PSA enhancer, whereas pol II was found predominantly in the elongating state at exon 5 (Fig. 6, *bottom*). In short, we show an example where AR has adapted to the androgen-deprived environment and resumed activity in the AI state as measured by gene expression-based imaging, immunohistochemistry, and ChIP.

DISCUSSION

AR Function in Recurrent Cancer. The natural response of prostate cancer to DHT withdrawal is transition to the recurrent state. In men, localized cancer can be treated surgically, but metastasized cancers become refractory to androgen withdrawal and resume

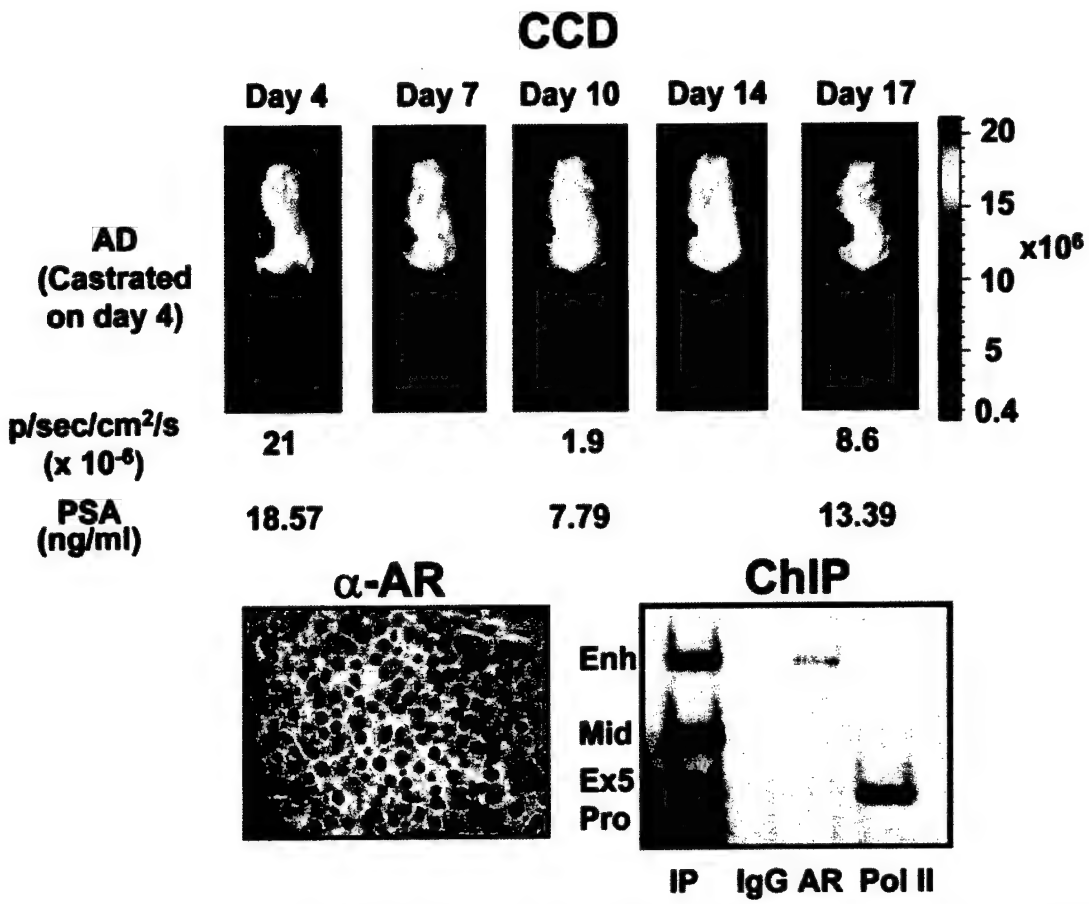

Fig. 6. Dynamic AR signaling. A SCID mouse bearing an LAPC9 AD tumor was injected with AdTSTA, imaged, and castrated. The *top panel* shows the entire time course with signals adjusted to the same color scale. Imaging measurements and PSA levels determined by serum ELISA are shown below the images. *Bottom left panel,* the tumors were extracted and subjected to immunohistological staining with AR antibodies. *Bottom right panel,* a ChIP assay of the extracted tumors with IgG, AR and pol II antibodies.

growth. The ability to recapitulate the transition to the recurrent state in xenograft models has provided a powerful tool for studying prostate tumor biology. The xenograft animals display the typical loss and then rise again in PSA levels upon castration. Although PSA is an AR-regulated gene, there have been proposals that other transcription factors may substitute for AR or that AR may be activating genes by a nongenotropic mechanism.

Three observations argue for a direct restoration of AR function. First, we redesigned the PSA transcriptional regulatory region to dramatically increase its response to AR. The modified PSA regulatory region was then built into a TSTA cassette to amplify its potency for use in live animal imaging. The imaging signals in recurrent tumors strongly suggest that AR is fully active. Furthermore, we could monitor the transition of an AD tumor to a recurrent state in a single individual, and visualize the loss and gain of AR activity during tumor progression. Second, immunohistochemistry on the xenograft tumors showed that AR localization was diffuse on androgen withdrawal but became tightly localized to the nucleus in recurrent tumors consistent with its role in DNA binding and transactivation. Finally, AR bound directly to the regulatory region of the PSA gene of AD tumors as measured by ChIP. Although the bulk of AR dissociated on castration it rebound again in stable AI and recurrent tumors. This last observation is particularly significant, because direct AR binding to a prostate-expressed gene has not been shown yet in advanced cancer.

Molecular Imaging of Prostate Cancer. The TSTA imaging scheme is a powerful approach to amplify weak cell-specific promoters and monitor their activity in live animals. By cloning the PSA-based TSTA cassette into adenovirus we generated a tool to monitor AR function during tumor progression from the AD to recurrent state. The AdTSTA system was designed to be particularly sensitive to AR by manipulating the enhancer region, which binds multiple molecules of AR cooperatively. The system responded dynamically and sensitively to castration of tumor-bearing mice. Typically, imaging signals decreased more rapidly than PSA levels, and the magnitude of the decrease was greater with the imaging system (10–20-fold) than PSA (2–3-fold). The short half-life of firefly luciferase (~12 h in the tumor) and the fact that it is an intracellular protein may have contributed to the enhanced sensitivity of the imaging signal. PSA is a secreted protein that exists both in the cell and serum. PSA half-life and secretion rates are likely to respond variably to the tumor environment and may not provide an immediate measure of AR activity.

The TSTA system is versatile and modular. We have now completed cloning of shuttle vectors in which the reporter gene can be replaced by any reporter (*e.g.,* thymidine kinase, green fluorescent protein, or *renilla* luciferase) or therapeutic gene for imaging or gene therapy. Furthermore, although we chose the modified PSA enhancer in our studies, the vector can accommodate any cell-specific or viral promoter. Finally, the system is titratable. In our previous cell culture study, which used plasmids, we systematically varied both the number of VP16 activation domains attached to GAL4 or the number of GAL4 sites driving the reporter. We were able to achieve a range of activities over 3 orders of magnitude. This variation should allow

optimization of signal:noise ratios and amplification of weak promoters for any application. Additionally, the vector is designed to replace the VP16 activation domain with domains that respond to signal transduction cascades. For example, we have successfully replaced VP16 with the activation domain of Elk-1 and shown that the system responds in a binary fashion to AR and signals emanating from the MAPK cascade.

On a technical note, there may be concerns about GAL4-VP16 and firefly luciferase toxicity. However, if toxicity was a significant issue we would predict that infected cells would die rapidly and the imaging signal would decay. However, under the conditions used in our study we were able to obtain persistent imaging signals in tumors over the course of the experiments, which can last up to a month. Also, the virus is not unusually toxic in cell culture, where cells appear to divide after infection. Our ability to use low doses of virus in the animal studies may permit a less immunogenic response and enable us to transit the system into non-SCID prostate models and transgenic animals.

Mechanism of AR Activation. The mechanism by which AR is reactivated in tumors has been the subject of much research and is commented on in the "Introduction." There are several interconnected issues including how does AR localize to the nucleus in the presence of castrate amounts of ligand, and how does it bind DNA and function in such an environment?

AR overexpression, ligand-binding domain mutations, and MAPK signaling have all been proposed as possible mechanisms to facilitate AR translocation and activity. Overexpression of SRC-1 and -2 coactivators has also been observed in some prostate tumors and may facilitate AR function. We have made two observations that bear on this issue. First, the AR levels in our recurrent tumors, when normalized to β-tubulin using a human specific antibody, are not dramatically higher than those in AD tumors (Supplementary Data, Fig. 3). We have also measured SRC-1, -2, and -3 levels, and they vary less than a few-fold among LAPC9 cancers. Thus, the localization of AR to the nuclei of recurrent tumors is not because of overexpression, which may bypass the normal cell trafficking checkpoints. Second, the AR gene in the LAPC9 tumor model has been sequenced and does not contain mutations in the ligand-binding domain, which might permit use of alternative ligands. Furthermore, if somehow the tumors were adapting to castration by hyperactivating pathways that convert adrenal androgen to DHT, we would have expected to see gradual increases in serum DHT over time. However, circulating levels of DHT in the LAPC9 mice drop up to 85% immediately after castration and remain at castrate levels throughout tumor growth. Finally, it is plausible that MAPK pathways are influencing AR translocation. We note that the particular tumor model we use, LAPC9, has been shown to display elevated EGF receptor and MAPK signaling (31).

Transcription Complex Assembly by AR. The binding of AR to the PSA enhancer paralleled increased serum PSA levels, the imaging signal, and AR cellular localization in both AD and AI cancer. Although AR-enhancer binding decreased 4-fold in ADc it increased again in AI cancer. As mentioned previously, PSA levels do not disappear completely in ADc but transiently plateau or drop as the tumors adapt. This observation can be explained by the fact that a subset of tumor cells from castrated animals still display AR nuclear localization and residual AR binding to the enhancer.

Although our data do not illuminate the precise mechanism of AR reactivation they provide insight into how the AD-AI transition may be facilitated. The most intriguing result is that although castration causes 75% of AR to dissociate from the PSA enhancer, the levels of bound TFIIB and pol II remain unchanged. However, castration did result in redistribution of pol II from exon 5 to the promoter. These observations suggest that transcription complexes do not disappear but remain poised to facilitate reactivation of AR-mediated transcription.

AR and pol II are known to cycle on and off the promoter during gene activation in LNCaP cells (15, 17). The peaks of AR and subsequent pol II binding after androgen addition do not coincide, suggesting that AR can leave while pol II is engaging the promoter. Analysis of genes such as α1-AT have also established that pol II can be bound with general factors such as TFIIB in a quiescent state, before binding of the activator (53). These data along with older studies of the heat shock locus in *Drosophila* (54) indicate that a prepoised pol II may provide a mechanism for maintaining promoter accessibility during a transcriptionally inactive state. The factors that control pol II redistribution are unknown. However, mutations in forkhead transcription factors in yeast are known to cause redistribution of pol II to the promoter (55). It is plausible that the poised complexes may be sensitive to lower levels of functional AR, thereby allowing activation in the absence of physiological levels of DHT. We are currently pursuing the mechanism of this effect.

ACKNOWLEDGMENTS

We thank Erika Billick for technical assistance during the early stages of the study, and Charles Sawyers and his laboratory for helpful discussions.

REFERENCES

1. Gelmann, E. P. Molecular biology of the androgen receptor. J. Clin. Oncol., *20:* 3001–3015, 2002.
2. Freedman, L. P. Increasing the complexity of coactivation in nuclear receptor signaling. Cell, *97:* 5–8, 1999.
3. Waller, A. S., Sharrard, R. M., Berthon, P., and Maitland, N. J. Androgen receptor localisation and turnover in human prostate epithelium treated with the antiandrogen, casodex. J. Mol. Endocrinol., *24:* 339–251, 2000.
4. Tyagi, R. K., Lavrovsky, Y., Ahn, S. C., Song, C. S., Chatterjee, B., and Roy, A. K. Dynamics of intracellular movement and nucleocytoplasmic recycling of the ligand-activated androgen receptor in living cells. Mol. Endocrinol., *14:* 1162–1174, 2000.
5. Bok, R. A., and Small, E. J. Bloodborne biomolecular markers in prostate cancer development and progression. Nat. Rev. Cancer, *2:* 918–926, 2002.
6. Pang, S., Taneja, S., Dardashti, K., Cohan, P., Kaboo, R., Sokoloff, M., Tso, C. L., Dekernion, J. B., and Belldegrun, A. S. Prostate tissue specificity of the prostate-specific antigen promoter isolated from a patient with prostate cancer. Hum. Gene Ther., *6:* 1417–1426, 1995.
7. Pang, S., Dannull, J., Kaboo, R., Xie, Y., Tso, C. L., Michel, K., deKernion, J. B., and Belldegrun, A. S. Identification of a positive regulatory element responsible for tissue- specific expression of prostate-specific antigen. Cancer Res., *57:* 495–499, 1997.
8. Schuur, E. R., Henderson, G. A., Kmetec, L. A., Miller, J. D., Lamparski, H. G., and Henderson, D. R. Prostate-specific antigen expression is regulated by an upstream enhancer. J. Biol. Chem., *271:* 7043–7051, 1996.
9. Cleutjens, K. B., van Eekelen, C. C., van der Korput, H. A., Brinkman, A. O., and Trapman, J. Two androgen response regions cooperate in steroid hormone regulated activity of the prostate-specfic antigen promoter. J. Biol. Chem., *271:* 6379–6388, 1996.
10. Cleutjens, K. B., van der Korput, H. A., van Eekelen, C. C., van Rooij, H. C., Faber, P. W., and Trapman, J. An androgen response element in a far upstream enhancer region is essential for high, androgen-regulated activity of the prostate-specific antigen promoter. Mol. Endocrinol., *11:* 148–161, 1997.
11. Cleutjens, K. B., van der Korput, H. A., Ehren-van Eekelen, C. C., Sikes, R. A., Fasciana, C., Chung, L. W., and Trapman, J. A 6-kb promoter fragment mimics in transgenic mice the prostate-specific and androgen-regulated expression of the endogenous prostate-specific antigen gene in humans. Mol. Endocrinol., *11:* 1256–1265, 1997.
12. Zhang, S., Murtha, P. E., and Young, C. Y. Defining a functional androgen responsive element in the 5′ far upstream flanking region of the prostate-specific antigen gene. Biochem. Biophys. Res. Commun., *231:* 784–788, 1997.
13. Huang, W., Shostak, Y., Tarr, P., Sawyers, C., and Carey, M. Cooperative assembly of androgen receptor into a nucleoprotein complex that regulates the prostate-specific antigen enhancer. J. Biol. Chem., *274:* 25756–25768, 1999.
14. Reid, K. J., Hendy, S. C., Saito, J., Sorensen, P., and Nelson, C. C. Two classes of androgen receptor elements mediate cooperativity through allosteric interactions. J. Biol. Chem., *276:* 2943–2952, 2001.
15. Kang, Z., Pirskanen, A., Janne, O. A., and Palvimo, J. J. Involvement of proteasome in the dynamic assembly of the androgen receptor transcription complex. J. Biol. Chem., *277:* 48366–48371, 2002.
16. Louie, M. C., Yang, H. Q., Ma, A. H., Xu, W., Zou, J. X., Kung, H. J., and Chen, H. W. Androgen-induced recruitment of RNA polymerase II to a nuclear receptor-p160 coactivator complex. Proc. Natl. Acad. Sci. USA, *100:* 2226–2230, 2003.

17. Shang, Y., Myers, M., and Brown, M. Formation of the androgen receptor transcription complex. Mol. Cell, *9:* 601–610, 2002.
18. Lee, C. T., and Oesterling, J. E. Diagnostic markers of prostate cancer: utility of prostate-specific antigen in diagnosis and staging. Semin. Surg. Oncol., *11:* 23–35, 1995.
19. Abate-Shen, C., and Shen, M. M. Molecular genetics of prostate cancer. Genes Dev., *14:* 2410–2434, 2000.
20. Arnold, J. T., and Isaacs, J. T. Mechanisms involved in the progression of androgen-independent prostate cancers: it is not only the cancer cell's fault. Endocr. Relat. Cancer, *9:* 61–73, 2002.
21. Feldman, B. J., and Feldman, D. The development of androgen-independent prostate cancer. Nat. Rev. Cancer, *1:* 34–45, 2001.
22. Gregory, C. W., Johnson, R. T., Jr., Mohler, J. L., French, F. S., and Wilson, E. M. Androgen receptor stabilization in recurrent prostate cancer is associated with hypersensitivity to low androgen. Cancer Res., *61:* 2892–2898, 2001.
23. Visakorpi, T., Hyytinen, E., Koivisto, P., Tanner, M., Keinanen, R., Palmberg, C., Palotie, A., Tammela, T., Isola, J., and Kallioniemi, O. P. *In vivo* amplification of the androgen receptor gene and progression of human prostate cancer. Nat. Genet., *9:* 401–406, 1995.
24. Stanbrough, M., Leav, I., Kwan, P. W., Bubley, G. J., and Balk, S. P. Prostatic intraepithelial neoplasia in mice expressing an androgen receptor transgene in prostate epithelium. Proc. Natl. Acad. Sci. USA, *98:* 10823–10828, 2001.
25. Gregory, C. W., He, B., Johnson, R. T., Ford, O. H., Mohler, J. L., French, F. S., and Wilson, E. M. A mechanism for androgen receptor-mediated prostate cancer recurrence after androgen deprivation therapy. Cancer Res., *61:* 4315–4319, 2001.
26. Han, G., Foster, B. A., Mistry, S., Buchanan, G., Harris, J. M., Tilley, W. D., and Greenberg, N. M. Hormone status selects for spontaneous somatic androgen receptor variants that demonstrate specific ligand and cofactor dependent activities in autochthonous prostate cancer. J. Biol. Chem., *276:* 11204–11213, 2001.
27. Grossmann, M. E., Huang, H., and Tindall, D. J. Androgen receptor signaling in androgen-refractory prostate cancer. J. Natl. Cancer Inst., *93:* 1687–1697, 2001.
28. Craft, N., and Sawyers, C. L. Mechanistic concepts in androgen-dependence of prostate cancer. Cancer Metastasis Rev., *17:* 421–427, 1998.
29. Elo, J. P., and Visakorpi, T. Molecular genetics of prostate cancer. Ann. Med., *33:* 130–141, 2001.
30. Gioeli, D., Mandell, J. W., Petroni, G. R., Frierson, H. F., Jr., and Weber, M. J. Activation of mitogen-activated protein kinase associated with prostate cancer progression. Cancer Res., *59:* 279–284, 1999.
31. Mellinghoff, I. K., Tran, C., and Sawyers, C. L. Growth inhibitory effects of the dual ErbB1/ErbB2 tyrosine kinase inhibitor PKI-166 on human prostate cancer xenografts. Cancer Res., *62:* 5254–5259, 2002.
32. Zegarra-Moro, O. L., Schmidt, L. J., Huang, H., and Tindall, D. J. Disruption of androgen receptor function inhibits proliferation of androgen-refractory prostate cancer cells. Cancer Res., *62:* 1008–1013, 2002.
33. Kousteni, S., Bellido, T., Plotkin, L. I., O'Brien, C. A., Bodenner, D. L., Han, L., Han, K., DiGregorio, G. B., Katzenellenbogen, J. A., Katzenellenbogen, B. S., Roberson, P. K., Weinstein, R. S., Jilka, R. L., and Manolagas, S. C. Nongenotropic, sex-nonspecific signaling through the estrogen or androgen receptors: dissociation from transcriptional activity. Cell, *104:* 719–730, 2001.
34. Peterziel, H., Mink, S., Schonert, A., Becker, M., Klocker, H., and Cato, A. C. Rapid signalling by androgen receptor in prostate cancer cells. Oncogene, *18:* 6322–6329, 1999.
35. Yeung, F., Li, X., Ellett, J., Trapman, J., Kao, C., and Chung, L. W. Regions of prostate-specific antigen (PSA) promoter confer androgen- independent expression of PSA in prostate cancer cells. J. Biol. Chem., *275:* 40846–40855, 2000.
36. Klein, K. A., Reiter, R. E., Redula, J., Moradi, H., Zhu, X. L., Brothman, A. R., Lamb, D. J., Marcelli, M., Belldegrun, A., Witte, O. N., and Sawyers, C. L. Progression of metastatic human prostate cancer to androgen independence in immunodeficient SCID mice. Nat. Med., *3:* 402–408, 1997.
37. Contag, C. H., Jenkins, D., Contag, P. R., and Negrin, R. S. Use of reporter genes for optical measurements of neoplastic disease *in vivo*. Neoplasia, *2:* 41–52, 2000.
38. Contag, P. R. Whole-animal cellular and molecular imaging to accelerate drug development. Drug Disc. Today, *7:* 555–562, 2002.
39. Herschman, H. R., MacLaren, D. C., Iyer, M., Namavari, M., Bobinski, K., Green, L. A., Wu, L., Berk, A. J., Toyokuni, T., Barrio, J. R., Cherry, S. R., Phelps, M. E., Sandgren, E. P., and Gambhir, S. S. Seeing is believing: non-invasive, quantitative and repetitive imaging of reporter gene expression in living animals, using positron emission tomography. J. Neurosci. Res., *59:* 699–705, 2000.
40. Massoud, T., and Gambhir, S. S. Molecular imaging in living subjects: Seeing fundamental biological processes in a new light. Genes Dev., *17:* 545–580, 2003.
41. O'Connell-Rodwell, C. E., Burns, S. M., Bachmann, M. H., and Contag, C. H. Bioluminescent indicators for *in vivo* measurements of gene expression. Trends Biotechnol., *20:* S19–S23, 2002.
42. Wu, J. C., Sundaresan, G., Iyer, M., and Gambhir, S. S. Noninvasive optical imaging of firefly luciferase reporter gene expression in skeletal muscles of living mice. Mol. Ther., *4:* 297–306, 2001.
43. Wu, L., Matherly, J., Smallwood, A., Adams, J. Y., Billick, E., Belldegrun, A., and Carey, M. Chimeric PSA enhancers exhibit augmented activity in prostate cancer gene therapy vectors. Gene Ther., *8:* 1416–1426, 2001.
44. Adams, J. Y., Johnson, M., Sato, M., Berger, F., Gambhir, S. S., Carey, M., Iruela-Arispe, M. L., and Wu, L. Visualization of advanced human prostate cancer lesions in living mice by a targeted gene transfer vector and optical imaging. Nat. Med., *8:* 891–897, 2002.
45. Iyer, M., Wu, L., Carey, M., Wang, Y., Smallwood, A., and Gambhir, S. S. Two-step transcriptional amplification as a method for imaging reporter gene expression using weak promoters. Proc. Natl. Acad. Sci. USA, *98:* 14595–14600, 2001.
46. Zhang, L., Adams, J. Y., Billick, E., Ilagan, R., Iyer, M., Le, K., Smallwood, A., Gambhir, S. S., Carey, M., and Wu, L. Molecular engineering of a two-step transcription amplification (TSTA) system for transgene delivery in prostate cancer. Mol. Ther., *5:* 223–232, 2002.
47. He, T. C., Zhou, S., da Costa, L. T., Yu, J., Kinzler, K. W., and Vogelstein, B. A simplified system for generating recombinant adenoviruses. Proc. Natl. Acad. Sci. USA, *95:* 2509–2514, 1998.
48. Pfeifer, A., and Verma, I. M. Gene therapy: promises and problems. Annu. Rev. Genomics Hum. Genet., *2:* 177–211, 2001.
49. Horoszewicz, J. S., Leong, S. S., Kawinski, E., Karr, J. P., Rosenthal, H., Chu, T. M., Mirand, E. A., and Murphy, G. P. LNCaP model of human prostatic carcinoma. Cancer Res., *43:* 1809–1818, 1983.
50. Tilley, W. D., Wilson, C. M., Marcelli, M., and McPhaul, M. J. Androgen receptor gene expression in human prostate carcinoma cell lines. Cancer Res., *50:* 5382–5386, 1990.
51. Montgomery, B. T., Young, C. Y., Bilhartz, D. L., Andrews, P. E., Prescott, J. L., Thompson, N. F., and Tindall, D. J. Hormonal regulation of prostate-specific antigen (PSA) glycoprotein in the human prostatic adenocarcinoma cell line, LNCaP. Prostate, *21:* 63–73, 1992.
52. Chen, C. D., and Sawyers, C. L. NF-κ B activates prostate-specific antigen expression and is upregulated in androgen-independent prostate cancer. Mol. Cell. Biol., *22:* 2862–2870, 2002.
53. Cosma, M. Ordered recruitment: gene-specific mechanism of transcription activation. Mol. Cell, *10:* 227–236, 2002.
54. Gilmour, D. S., and Lis, J. T. RNA polymerase II interacts with the promoter region of the noninduced hsp70 gene in Drosophila melanogaster cells. Mol. Cell. Biol., *6:* 3984–3989, 1986.
55. Morillon, A., O'Sullivan, J., Azad, A., Proudfoot, N., and Mellor, J. Regulation of elongating RNA polymerase II by forkhead transcription factors in yeast. Science (Wash. DC), *300:* 492–495, 2003.

tapraid3/c4-mthe/c4-mthe/c41103/c41093d03a | knepperl | S=5 | 9/18/03 | 7:56 | Art: 1093

doi:10.1016/j.ymthe.2003.08.016

ARTICLE

Optimization of Adenoviral Vectors to Direct Highly Amplified Prostate-Specific Expression for Imaging and Gene Therapy

Makoto Sato,[1] Mai Johnson,[1] Liqun Zhang,[2] Baohui Zhang,[1] Kim Le,[2] Sanjiv S. Gambhir,[3*] Michael Carey,[2,3] and Lily Wu[1,3,†]

[1]*Department of Urology,* [3]*Crump Institute of Molecular Imaging and Department of Molecular and Medical Pharmacology, and* [2]*Department of Biological Chemistry, University of California at Los Angeles School of Medicine, Los Angeles, California 90095*

**Present address: Department of Radiology and Bio-X Program, Stanford University, Stanford, CA.*

†To whom correspondence and reprint requests should be addressed. Fax: (310) 206-5343. E-mail: LWu@mednet.ucla.edu.

Gene expression-based imaging coupled to gene therapy will permit the prediction of therapeutic outcome. A significant challenge for successful gene therapy is to achieve a high-level of specific gene expression; however, tissue-specific promoters are weak. We postulate that if the weak activity of tissue-specific promoters can be amplified to the levels of strong viral promoters, which have been successful in preclinical scenarios, while retaining specificity, the therapeutic index of gene therapy can be greatly augmented. With this in mind, we developed a two-step transcriptional activation (TSTA) system. In this two-tiered system, a modified prostate-specific antigen promoter was employed to drive a potent synthetic transcriptional activator, GAL4-VP2. This, in turn, activated the expression of a GAL4-dependent reporter or therapeutic gene. Here we demonstrate that recombinant adenoviral vectors (Ads) in which we have incorporated prostate-targeted TSTA expression cassettes retain cell specificity and androgen responsiveness in cell culture and in animal models, as measured by noninvasive optical bioluminescence imaging. We investigated the mechanism of TSTA in different adenoviral configurations. In one configuration, both the activator and the reporter components are inserted into a single Ad (AdTSTA-FL). The activity of AdTSTA-FL exceeds that of a cytomegalovirus promoter-driven vector (AdCMV-FL), while maintaining tissue specificity. When the activator and reporter components are placed in two separate Ads, androgen induction is more robust than for the single AdTSTA-FL. Based on these findings, we hope to refine the TSTA Ads further to improve the efficacy and safety of prostate cancer gene therapy.

Key Words: prostate-specific expression, two-tiered amplification, androgen regulation, adenoviral vector, optical imaging

INTRODUCTION

Metastatic and recurrent hormonal refractory prostate cancer (HRPC) account for an estimated loss of one life every 17 minutes in the United States [1]. Androgen ablation is the main treatment for advanced disease and can induce an initial remission and achieve symptomatic improvement in 80–90% of patients [2–4]. However, progression to HRPC is inevitable even in the absence of circulating androgen. Currently, there is no effective treatment for HRPC, and median survival is approximately 12 months. Gene-based therapy is a promising possibility for HRPC [5,6]. However, an important prerequisite for developing a safe and effective therapy is to achieve high levels of prostate-specific gene expression *in vivo* [6].

The use of tissue-specific promoters to express transgenes is an attractive approach that is particularly suitable for prostatic tissue, because it is one of the organs other than the pancreas and breast that expresses an unusually high number of unique genes. A survey of the Cancer Genome Anatomy Project database published by the National Cancer Institute (http://www.ncbi.nlm.nih.gov/ncicgap/) lists more than 2000 prostate-specific genes, although the majority of them are not fully characterized at this time. Many prostate-specific genes, including pros-

1525-0016/03 $30.00

ARTICLE

doi:10.1016/j.ymthe.2003.08.016

tate-specific antigen (PSA) and prostate-specific membrane antigen, are well characterized [7–12]. The PSA gene is regulated by testosterone (T) and dihydrotestosterone (DHT), which bind androgen receptor (AR). The ligand-bound AR binds directly to sites within the PSA promoter and enhancer, thus activating PSA gene expression [7,10,11]. Clinical findings indicate that AR and PSA are expressed in all stages of prostate cancer and in distant metastases, even after androgen-deprivation therapy [13–16]. Currently, serum PSA measurements remain the most reliable means to detect recurrent HRPC [17]. Numerous studies support the likelihood that the AR pathway is still functioning in HRPC at castrated levels of DHT and T. Several mechanisms have been proposed to facilitate AR function under androgen-deprived conditions [6,18], such as AR overexpression [19]; increased expression of the nuclear receptor transcriptional coactivators, SRC-1 and SRC-2 [20]; AR mutations that confer expanded ligand specificity [21]; or cross talk between other signaling cascades and AR pathways [22].

We were interested in generating systems for delivery of therapeutic and imaging genes to prostate cancer. We designed our systems around the PSA promoter because of its ability to function in early androgen-dependent prostate cancer and in advanced-stage HRPC [23] and metastasis. Although the native PSA regulatory elements confer tissue selectivity, their activity is too weak to mediate efficient vector-based gene expression *in vivo* [6]. Therefore, we have undertaken two strategies to augment the activity of the PSA promoter/enhancer, while maintaining its specificity. First, the upstream enhancer core of PSA was duplicated in a construct designated PSE-BC, which achieved 20-fold enhancement of activity compared to the native PSA enhancer and promoter construct [24,25]. An adenoviral vector (Ad) bearing this PSE-BC promoter-driven firefly luciferase (FL) gene was able to achieve targeted expression in distant metastatic prostate cancer cells in living mice [26]. In a second approach, we employed a two-step transcriptional amplification (TSTA) system both to elevate and to modulate the activity of the PSA enhancer/promoter over a 1000-fold range [27,28]. In this two-tiered system illustrated in Fig. 1a, the PSA regulatory region was employed to express the potent synthetic transcription activator, GAL4-VP2, which in turn activates a GAL4-responsive reporter. In tissue culture transfection studies, optimal TSTA constructs displayed levels of activity significantly higher than the cytomegalovirus immediate early promoter (CMV), while maintaining prostate cell specificity and ligand responsiveness [27,28].

Imaging of vector-mediated transgene expression provides a critical assessment of the *in vivo* capabilities of targeted gene transfer. Rapid advances in imaging technology have allowed repetitive monitoring of the location, magnitude, and kinetics of reporter gene expression in small living animals [29–31]. Optical bioluminescence imaging (BLI) is particularly suitable for small animal studies, with the distinct advantage of low background signal, rapid scanning time, and low cost in comparison to radionuclide imaging. The *in vivo* expression of the popular FL reporter gene can be monitored by a highly sensitive cooled charge-coupled device (CCD) camera after the administration of the relatively nontoxic d-luciferin substrate in living animals [32,33]. Because imaging can provide real-time information on *in vivo* biological processes, the BLI technology was used to monitor estro-

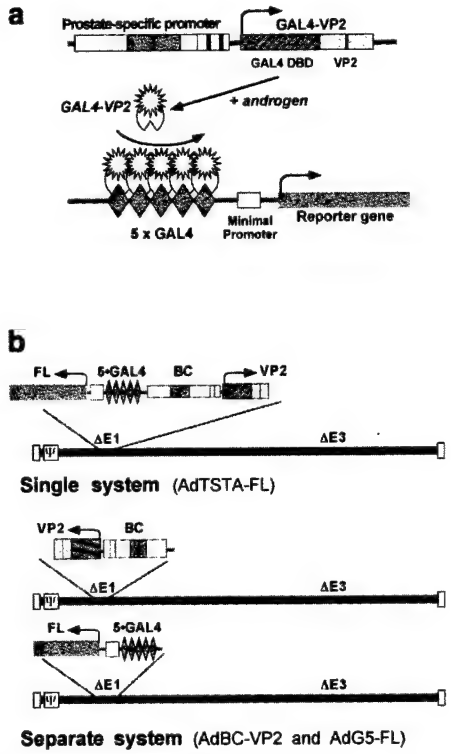

FIG. 1. Schematic representation of TSTA system. (a) Illustration of the two-step transcriptional activation process. In the first step, GAL4-VP2 activator proteins (fusion of GAL4 DNA binding domain and two copies of the VP16 transactivation domain) are expressed under the control of a prostate-specific promoter (an augmented PSA promoter, PSE-BC), which is activated by androgen. In the second step, GAL4-VP2 binds to a GAL4-responsive promoter and activates the expression of the FL reporter gene. (b) The two different TSTA configurations in Ad. In the single TSTA Ad (AdTSTA-FL), both activator and reporter are inserted into the E1 region of the same Ad in a head-to-head orientation. In the separate TSTA Ads (AdBC-VP2 and AdG5-FL), activator and reporter components are incorporated into the E1 region of two separate Ads with the transcription oriented toward the left end of the viral genome. BC is the abbreviation of the PSE-BC prostate-specific promoter [25]. ψ denotes the packaging signal of adenovirus and open rectangles at both termini denote inverted terminal repeats of the viral genome.

doi:10.1016/j.ymthe.2003.08.016

gen receptor function under physiological conditions and during pharmacological intervention [34].

To assess the potential of the TSTA system in gene therapy applications, we incorporated the system into an Ad, which is an efficient *in vivo* gene delivery vehicle. The purpose of this study was to investigate the *in vivo* specificity of and the parameters necessary to achieve optimal regulation of the TSTA system in different Ad configurations. In the AdTSTA-FL construct, the activator and reporter component were inserted into the Ad in a divergently linked head-to-head configuration. Alternatively, two Ads that separately express the GAL4-responsive FL and the PSE-BC-regulated GAL4-VP2 activator were also generated. We analyzed the prostate-specific expression and androgen regulation of the separate TSTA Ads in comparison to the single AdTSTA-FL *in vitro* and *in vivo*. We found that separate Ads elicited a more robust response to androgen versus the single Ad.

RESULTS

Generation of Adenovirus Vectors Containing the TSTA System

The TSTA system is schematically represented in Fig. 1a. We previously determined the combination of activator and reporter plasmid TSTA constructs that achieves the highest levels of activity in prostate cancer cells using transfection studies [28]. Based on these results, we generated TSTA Ads, utilizing the bacterial recombination AdEasy methodology [35]. The activator is composed of an augmented prostate-specific PSE-BC promoter/enhancer [25] controlling the expression of the chimeric activator protein, GAL4-VP2 (the GAL4 DNA-binding domain fused to two tandem repeats of the herpes simplex virus VP16 activation domain) [28]. The reporter component consists of five repeats of the 17-bp GAL4 binding sites positioned upstream of a minimal promoter containing the adenovirus E4 gene TATA box driving FL. We inserted the activator (BC-VP2) and reporter (G5-FL) components linked in a divergent head-to-head orientation into the E1 region of the Ad, resulting in the AdTSTA-FL vector (Fig. 1b). We also constructed two Ads, designated AdBC-VP2 and AdG5-FL, which harbor the BC-VP2 activator and the G5-FL reporter, respectively (Fig. 1b).

Specificity of the TSTA Vectors

We evaluated the capability of AdTSTA-FL to direct prostate-specific expression by infecting a variety of cell lines derived from different tissues. Human serotype 5 Ad exhibits wide cell-type viral tropism. However, the susceptibility of a cell line to Ad infection is modulated by the cell surface expression of coxsackievirus and adenovirus receptor (CAR) [36,37] and αv integrins [38]. Thus, a measurement of infectivity in different cell lines is needed to assess the activity of AdTSTA-FL. Initially, we determined relative infectivity of different cells by normalization to the activity of AdCMV-FL, in which the FL expression is driven by the constitutively active CMV promoter. Our view was that similar pfu (plaque-forming unit) amounts of AdTSTA-FL and AdCMV-FL should display similar infectivity. Thus, differences in the activity of AdCMV-FL in different lines would represent a standard for normalizing infectivity of AdTSTA-FL. However, two findings alerted us to the potential inaccuracy of this measurement: (1) a 3- to 4-fold androgen induction was noted in the AdCMV-FL-infected prostate cell lines (data not shown) and (2) a greater than 30-fold difference in activity was observed between the most and the least active cell lines infected with equivalent doses of AdCMV-FL (data not shown). Discrepancy between luciferase activity and physical viral DNA measurement mediated by AdCMV-luc in different cell types has been reported [39]. An ideal assay to measure infectivity is not available.

In this study we elected to use the viral DNA uptake in the cells as a measurement of infectivity. We harvested the internalized viral DNA from infected cells and quantified the FL DNA by real-time PCR. We determined the infectivities of LNCaP and LAPC-4 (prostate carcinoma), H157 and A549 (lung cancer), MCF-7 (breast carcinoma), HepG2 (liver cancer), and HeLa (cervical carcinoma) cell lines by this viral DNA uptake approach. Among the panel of cell lines that we tested, HeLa cells were the least susceptible to infection and their infectivity was designated as 1. The infectivities of LNCaP, H157, A549, MCF7, LAPC-4, and HepG2 cells were 1.7-, 1.6-, 1.5-, 1.3-, 1.1-, and 1.1-fold higher than that of HeLa cells, respectively. Differential CAR expression in different stages of prostate carcinoma [40] might contribute to the enhanced infection in LNCaP cells.

We evaluated the activity of AdTSTA-FL in several prostate cancer cell lines, including two androgen-responsive cell lines (LNCaP and LAPC-4 [41]) and two AR-negative lines (DU145 and PC-3). Infection was carried out at a calculated AdTSTA-FL dosage of 1 infectious unit (pfu) per cell (m.o.i. 1). The normalized FL activity in LAPC-4 was 4.4-fold lower than LNCaP (see Fig. 5b and data not shown). Conversely, the FL activity in AR-negative prostate cancer lines was negligible (nearly 500-fold lower than in LNCaP cells, data not shown). For simplicity, we compared the normalized FL activities to that of the LNCaP cell line, set at 100% (Fig. 2a). The activity in A549, H157, HepG2, HeLa, and MCF7 cells was 290-, 1200-, 4500-, 6000-, and 20,000-fold lower than in LNCaP cells, respectively (Fig. 2a). The FL activity in nonprostate cell lines and AR-negative prostate cancer lines was not induced by androgen (data not shown). We also observed consistent diminished cell-specific expression in infections. At higher m.o.i. the cell specificity became less apparent due to higher androgen-independent or basal activity, an effect that we do not completely understand (data not shown). For example, AdTSTA-FL-mediated activity in HeLa cells at m.o.i. 10 was 660-fold lower than in

doi:10.1016/j.ymthe.2003.08.016

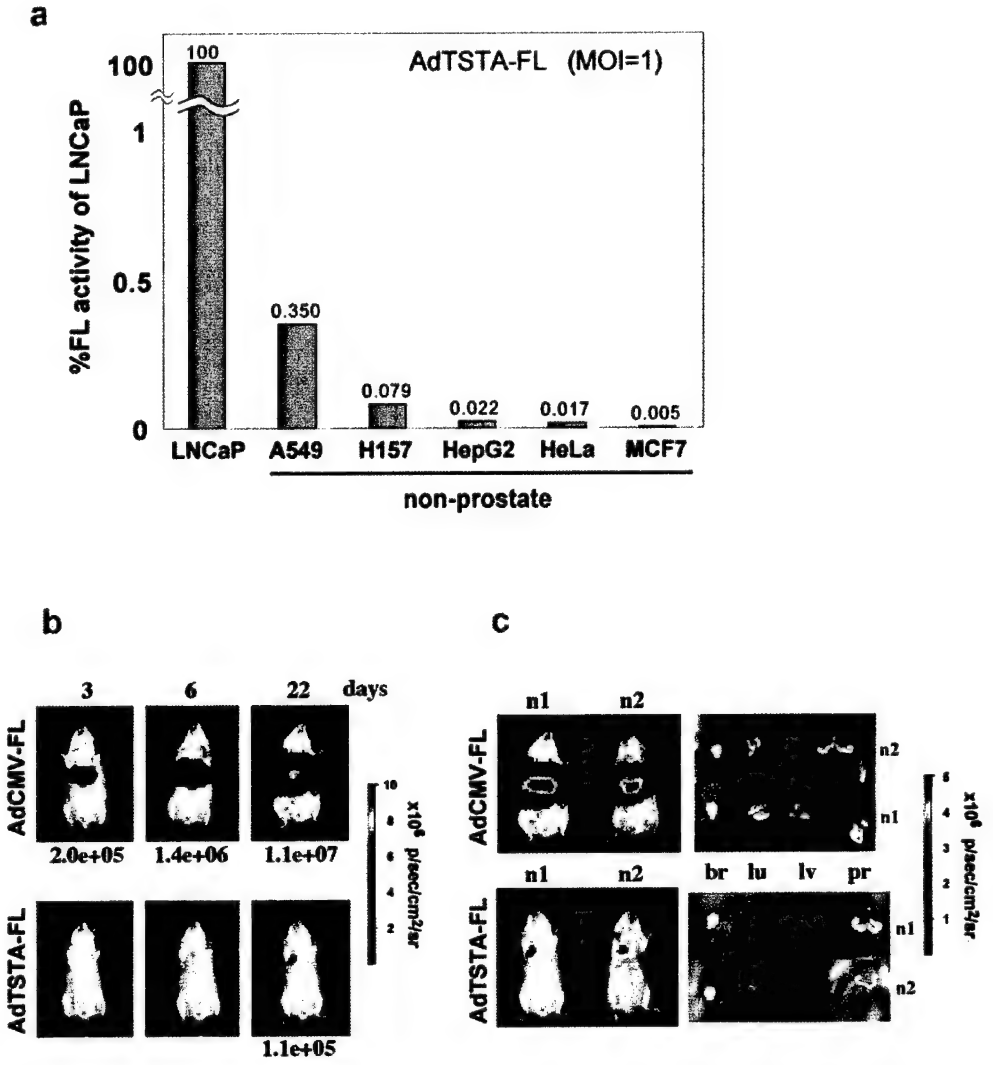

FIG. 2. Cell specificity of the TSTA Ad. (a) *In vitro* cell specificity of AdTSTA-FL. The prostate cell line LNCaP and nonprostate cell lines were infected with AdTSTA-FL at m.o.i. 1. Cells were harvested and subjected to an FL assay 48 h after infection. FL activity was normalized to cell numbers and infectivity of each cell line as assayed by real-time PCR (see Materials and Methods). FL activity was plotted for each cell line using LNCaP (an androgen-responsive prostate carcinoma line) as a normalization standard, set at 100%. The activities in nonprostate cell lines are more than 290-fold lower than in LNCaP. (b) *In vivo* tissue specificity of AdTSTA-FL. 10^7 pfu (plaque-forming units = infectious units) of Ad was injected into naïve mice via the tail vein and FL expression was sequentially monitored by optical imaging at days 3, 6, and 22. Robust liver signals were noted in the AdCMV-FL-injected animals starting at day 3 and increasing from that point onward. The AdTSTA-FL-injected animals remained transcriptionally silent until day 22, when a weak signal was noted in the lung. Numbers below the images are the maximal activities in the region of interest as photons (p) acquired per second per square centimeter per steridan (sr). (c) Optical activities in the isolated organs. Two additional animals (n1 and n2) from the AdCMV-FL- or AdTSTA-FL-injected group were sacrificed at day 22, and the isolated organs were reimaged. The liver is the predominant site of expression in AdCMV-FL-injected animals. Low level of expression in the lung was observed in the AdTSTA-FL-injected animals (br, brain; lu, lung; lv, liver; and pr, prostate).

LNCaP cells, compared to 6000-fold at m.o.i. 1 (data not shown; see Discussion).

We next investigated the specificity of the single AdTSTA-FL *in vivo*. We compared its activity to that of AdCMV-FL, because vector DNA quantitation studies in animals are less well controlled. We employed CCD imaging to monitor *in vivo* expression over a 22-day period. Fig. 2b illustrates the optical imaging profiles of animals that received systemic administration of AdTSTA-FL or AdCMV-FL. A robust signal emanating from the midsection

doi:10.1016/j.ymthe.2003.08.016

ARTICLE

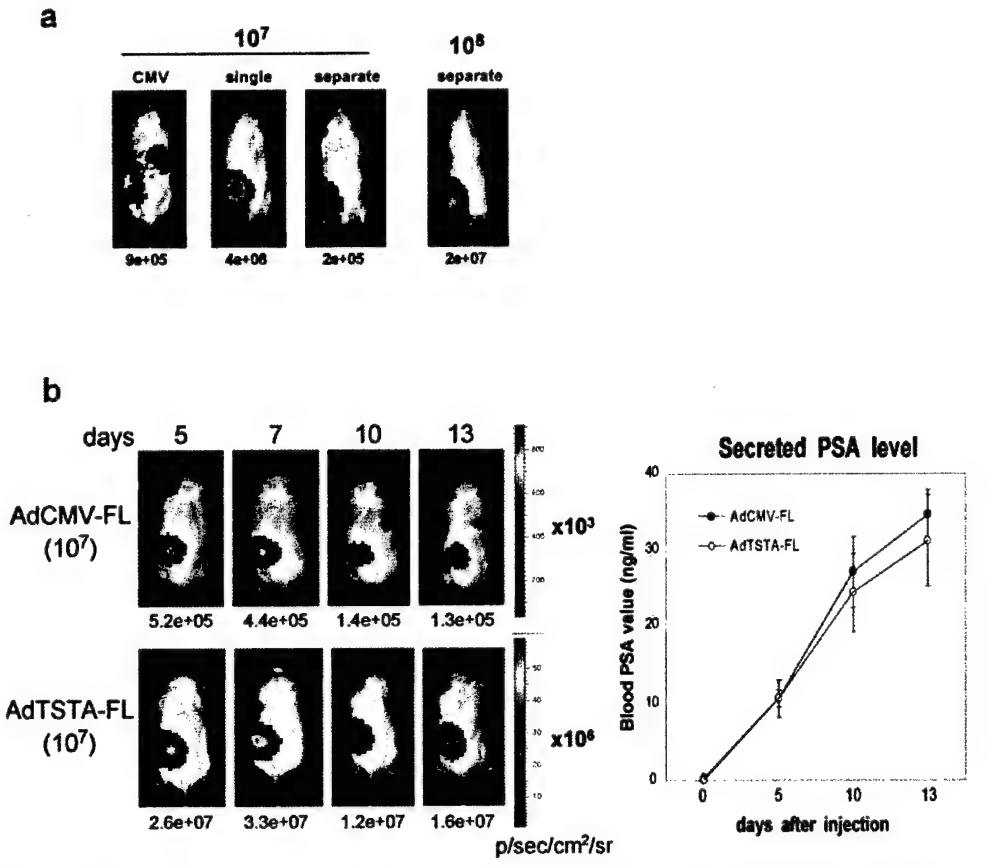

FIG. 3. *In vivo* FL expression mediated by single and separate TSTA Ads in LAPC-4 xenografts and prostates. (a) Optical signals after injections of the respective Ads in LAPC-4 tumors. 10^7 or 10^8 pfu of Ads (as specified) was injected. The injection of separate Ads denotes the coadministration of both AdBC-VP2 and AdG5-FL at the specified dosage. CCD images of representative animals analyzed at 4 days postinjection were shown. (b) Kinetics of FL expression in LAPC-9 tumors. 10^7 pfu of AdCMV-FL or AdTSTA-FL was injected intratumorally. Optical signals were monitored on the specified days after viral injection. The number below each image represents the maximal signal over the tumor. The graph on the right represents the averaged serum PSA level measured in the animals at the specified days post-viral injection.

of mice injected with AdCMV-FL via the tail vein was seen as early as 3 days postinjection, which we determined was due to efficient liver transduction as assessed by imaging of isolated organs (Figs. 2b and 2c). In contrast, the AdTSTA-FL-injected animals did not have detectable signals until a late time point (day 22), which signals then appeared in the lung (Figs. 2b and 2c); however, this signal is more than 3 orders of magnitude lower than tumor-directed expression (see Fig. 3). The absence of optical signal in the prostate after tail vein injection of AdTSTA-FL is unclear at this time. However, limitations of *in vivo* Ad distribution that result in low gene transfer to organs other than mouse liver have been well documented [42]. We expand on these issues under Discussion.

We next evaluated intratumoral activity mediated by both single and separate TSTA Ads in LAPC-4 xenografts, which were derived from a lymph node metastatic lesion from a patient [41]. LAPC-4 expresses PSA and AR and exhibits androgen-responsive gene expression and growth. Fig. 3a shows that intratumoral injection of 10^7 pfu of the single AdTSTA-FL resulted in a robust signal at 4 days postinjection, compared to AdCMV-FL. In a cohort of four animals, the average activity of AdTSTA-FL was 110-fold higher than that seen with AdCMV-FL ($P = 0.06$).

Cancer-specific gene therapy based on activation of a toxic gene by the Cre/lox recombination system delivered by separate two Ads has been reported to work in animals [43,44]. However, *in vivo* transduction of the two paired TSTA Ads, AdBC-VP2 and AdG5-FL, into the same cell, is anticipated to be less effective than delivery of a single

ARTICLE doi:10.1016/j.ymthe.2003.08.016

vector containing both elements. Thus, it is not surprising that injection of 10^7 pfu of each of the two Ads resulted in lower optical signal (2×10^5 photons/s/cm^2/sr) versus single Ad (4×10^8 photons/s/cm^2/sr). When the dose of the two paired TSTA Ads was increased to 10^8 pfu each, expression level (2×10^7 photons/s/cm^2/sr) higher than that of 10^7 pfu of AdCMV-FL (9×10^5 photons/s/cm^2/sr) was achieved (Fig. 3a). However, this magnitude of activity is still lower than can be achieved by 10^7 pfu of AdTSTA-FL (4×10^8 photons/s/cm^2/sr).

We examined the kinetics of expression after intratumoral delivery of 10^7 pfu of AdCMV-FL and AdTSTA-FL into LAPC-9 tumors. The LAPC-9 xenograft expresses AR and PSA and was derived from a bone metastasis [41]. Sequential optical images between 5 and 13 days postviral injection were recorded (Fig. 3b). The TSTA vector displayed 50- to 100-fold higher levels of FL activity than the AdCMV-FL during this period (Fig. 3b). The increasing serum PSA levels in both groups likely reflect the increase in tumor mass over the duration of the time course (Fig. 3b, right). However, despite the consistent increase in serum PSA levels the intratumoral FL signals gradually decayed after day 7 in both the AdCMV and the AdTSTA cohorts (Fig. 3b) due to the transient nature of Ad-mediated gene expression. The LAPC-9 tumors, like the LAPC-4 tumors, show a propensity for vector leakage into systemic circulation. However, we consistently observed a greater magnitude of leakage in LAPC-4 tumors, which was manifested as prominent signals in the liver after intratumoral injection of AdCMV-FL [26]. Because both vectors (TSTA and CMV) are serotype 5 adenovirus with the same deletion of the E1 and E3 genes, their biodistribution in mice should not differ. Intratumoral injection of AdTSTA-FL should result in the same extent of vector leakage as AdCMV-FL. However, no detectable liver signal was observed after intratumoral injection of AdTSTA-FL. This finding supports our view that the prostate specificity of TSTA is able to prevent expression of FL in the liver.

Androgen Regulation of the TSTA Ads

To determine if TSTA Ads respond to androgen regulation *in vivo* we assessed FL expression in the prostates of intact and castrated male SCID mice (Fig. 4). We injected 10^6 pfu of AdTSTA-FL or 10^8 pfu each of AdBC-VP2 and AdG5-FL into the prostate glands of cohorts of either intact male mice or mice castrated 7 days prior to injection (androgen-deprived group). The intact males infected with the single- or two-virus TSTA vectors displayed significant optical signals compared to the castrated mice. We conclude that both vector systems are responding to androgen depletion *in vivo* (Fig. 4a). The FL expression level of a 100-fold higher dose of the separate TSTA Ads was 20-fold greater than that of the single AdTSTA-FL (Fig. 4a, graphs). We also observed androgen regulation of AdTSTA-FL in the prostate gland when castration was performed 30 days postinjection, after FL expression had stabilized. In this case a 3-fold drop in expression was observed 3 days after castration (Fig. 4b).

To investigate androgen regulation of the TSTA Ads in more detail, we employed cell culture infection studies, in which the concentration of androgen and its antagonists could be carefully manipulated. We infected two androgen-dependent prostate cancer cell lines, LNCaP and LAPC-4, with TSTA Ads at different m.o.i. and androgen concentrations. Androgen levels in the medium were manipulated by adding R1881 (methylenetrienolone), a synthetic androgen that is more stable than DHT under culture conditions. The antagonist Casodex was used to minimize residual androgen activity in the charcoal-stripped serum because even low androgen levels activate the highly sensitive TSTA system. Both the activator and the reporter TSTA components are required to generate detectable FL in the two-virus system (Fig. 5a). Additionally, androgen stimulated the FL activity for both the separate and the single TSTA Ads, with the highest activity observed between 1 and 10 nM R1881. In Fig. 5b, AdTSTA-FL demonstrates a clear m.o.i.- and R1881-dependent increase in FL activity. In the presence of 1 nM R1881, activity increased 27-fold from m.o.i. 0.1 to m.o.i. 1 in LNCaP cells and 96-fold from m.o.i. 1 to m.o.i. 10 in LAPC-4 cells.

We also quantitated the androgen response of TSTA Ads by calculating the fold induction, based on the ratio of the highest activity at 10 nM R1881 over the basal activity in the presence of Casodex. Both separate and single TSTA Ads exhibited high levels of androgen induction in LNCaP and LAPC-4 cells. The androgen induction observed in infections at m.o.i. 1 and 5 of separate Ads were 672- and 915-fold, respectively, in LNCaP cells, and 52- and 67-fold, respectively, in LAPC-4 cells. The androgen induction mediated by the single AdTSTA-FL was 117- and 101-fold at m.o.i. 1 and 5 in LNCaP cells, respectively, and 35- and 24-fold in LAPC-4 cells at m.o.i. 1 and 5, respectively. The single AdTSTA-FL displayed diminished androgen inducibility compared to separate TSTA Ads. This point is illustrated in Fig. 5c by a plot of the relative induction ratio of separate Ads to single AdTSTA-FL in LNCaP and LAPC-4 cells at the two different m.o.i. The lower inducibility of AdTSTA-FL is not due to a lower maximal activity, but to a higher basal activity (in the presence of Casodex). Because this higher basal activity could potentially contribute to reduced specificity, we investigated the activation mechanism of TSTA Ads in more detail.

Investigating the Activation Mechanism in Single and Separate TSTA Ads

To investigate the mechanism responsible for differences in androgen induction, we analyzed FL activity and activator protein expression profiles over a wide range of infection ratios. LNCaP cells were infected with AdT-

doi:10.1016/j.ymthe.2003.08.016

ARTICLE

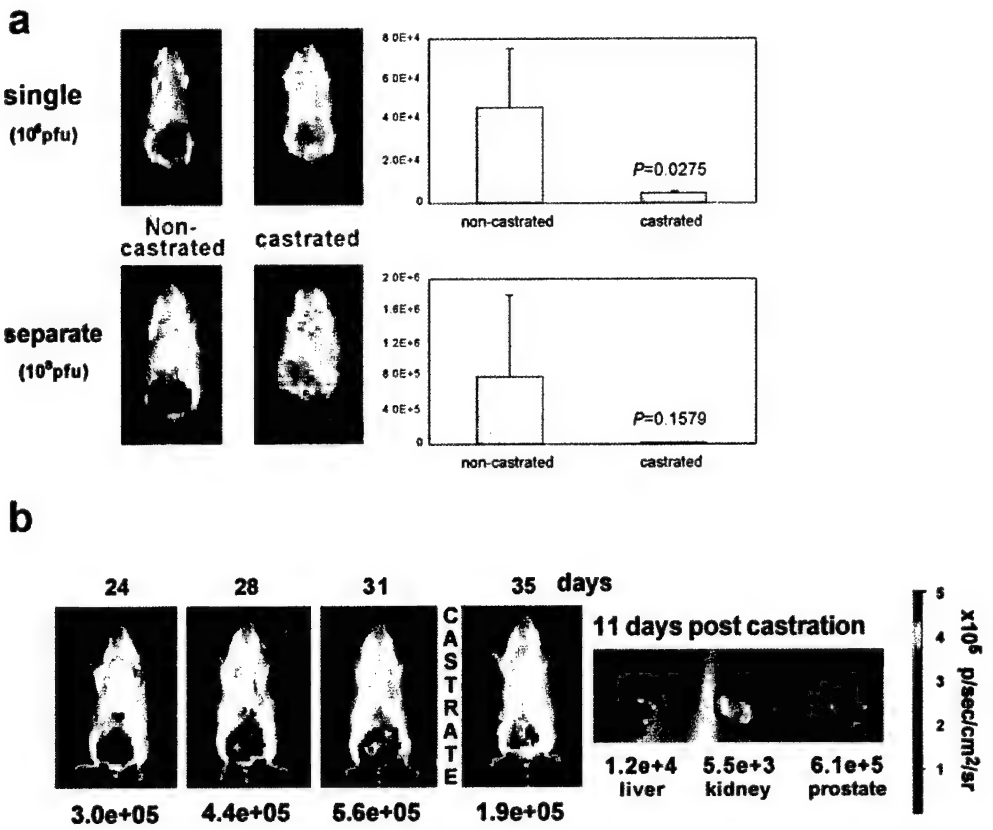

FIG. 4. Intraprostatic signals in intact and castrated animals. (a) AdTSTA-FL (10^6 pfu) or AdBC-VP2 and AdG5-FL (10^8 pfu each) were injected into the prostate of intact and castrated male SCID (7-days postcastration). The images were taken 4 days after viral injection. In each group, n is ≥ 3 animals. The averages and standard errors are plotted on the right. The FL signals in the castrated animals were 4.7×10^3 and 9.6×10^3 with single and separate TSTA Ad, respectively. The significance between intact and castrated animals is denoted in each graph as the P value. (b) The FL signal mediated by AdTSTA-FL in the same animal before and after castration. 10^7 pfu of AdTSTA-FL was injected into prostate in intact SCID mice. Days post-intraprostatic viral injection are indicated above the mouse images. The animal was castrated at day 31 and reimaged at day 35 (4 days postcastration). The animal was sacrificed at 11 days postcastration (day 42). The prostate gland was the predominant site of expression. The optical activity is specified below each image.

COLOR

STA-FL at m.o.i. of 50, 16.7, 5.6, 1.9, 0.62, and 0.21 (threefold serial dilutions). For the separate system, we added AdBC-VP2 and AdG5-FL at the indicated m.o.i. to generate levels of activator and reporter gene delivery equivalent to those in the single AdTSTA-FL infections. We demonstrated by Southern blotting that equal m.o.i. of AdTSTA-FL and AdBC-VP2 led to equivalent amounts of vector delivery (data not shown). We then examined FL activity and activator expression 48 h postinfection, as shown in Fig. 6. It is difficult to compare directly the levels of FL activity of single and separate Ad infections, especially at low m.o.i., due to the limited codelivery. However, both systems exhibited m.o.i.-dependent increases in activity as indicated in earlier figures. We observed a saturation of activity in both single and separate TSTA vectors. Overall, the magnitude of FL activity corresponded very well with the level of GAL4-VP2 expression measured by Western blotting. In the single AdTSTA-FL infections, the GAL4-VP2 expression reached a maximum at m.o.i. 16.7. We did not observe a plateau of activator expression in the separate TSTA infections at the range of m.o.i. tested. A surprising finding was that at each m.o.i., the activator expression in the single AdTSTA-FL was considerably higher than that mediated by the AdBC-VP2 in the separate system, despite comparable levels of activator (BC-VP2) gene delivery (data not shown). Given the fact that the same PSE-BC promoter-driven GAL4-VP2 expression cassette was inserted into both the single and the separate TSTA Ads, the different protein levels observed imply that a property of the vector genome context or design is influencing GAL4-VP2 expression. We propose in the Discussion that a self-perpetuating feedforward loop may be activated by the head-to-head orientation of AdTSTA-FL. A positive feedback loop could explain the

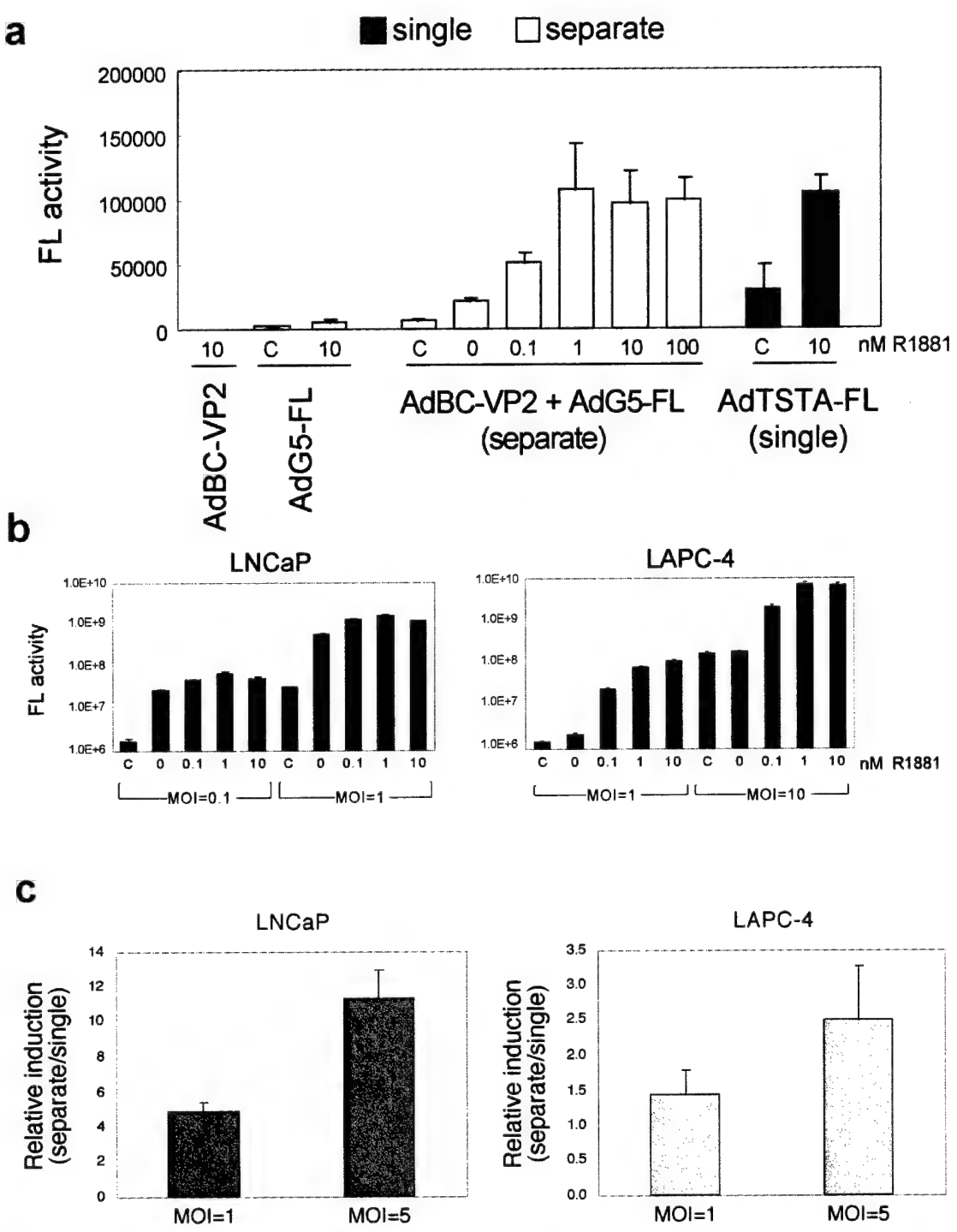

FIG. 5. *In vitro* expression and regulation of the single and separate TSTA Ads. (a) Expression of TSTA Ads in LAPC-4. LAPC-4 cells were infected with Ad at m.o.i. 10. 48 h postinfection the cells were harvested and assayed. Infections with AdBC-VP2 or AdG5-FL exhibited minimal activity. The FL activities of co-infection of separate TSTA Ads increased with increasing amount of synthetic androgen (R1881, nM). C denotes the addition of 10 μM Casodex (anti-androgen). (b) Androgen regulation of AdTSTA-FL. LNCaP and LAPC-4, two androgen-dependent prostate cell lines, were infected with AdTSTA-FL at the indicated m.o.i. in the presence of Casodex or R1881. The FL activities assayed at 48 h postinfection are shown. (c) Relative androgen induction ratio of the separate to the single TSTA Ads. The cells were infected at m.o.i. 1 or 5. Fold induction of activity was calculated based on the ratio of the peak activity (in 10 nM R1881) to the basal activity (in 10 μM Casodex). The relative induction ratio was calculated by dividing the androgen induction in the separate TSTA Ads infection by the induction in the single-AdTSTA-FL-infected cells. The ratio shows that separate TSTA Ads exhibit higher androgen induction than the single Ad.

doi:10.1016/j.ymthe.2003.08.016

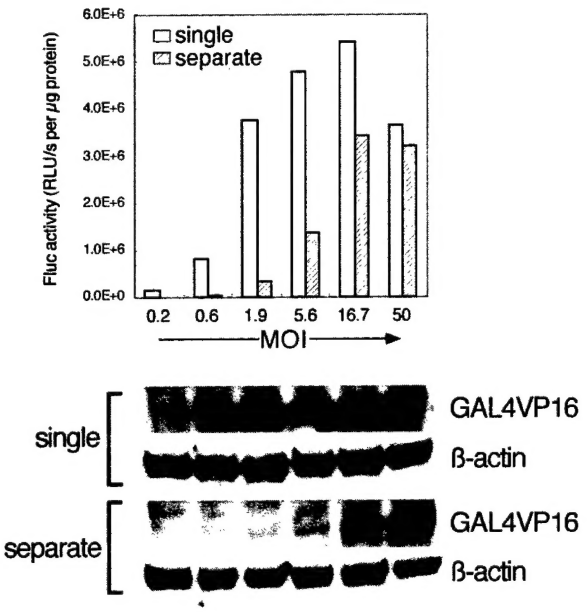

FIG. 6. The activation mechanism in TSTA Ads. LNCaP cells were infected with AdTSTA-FL at specified m.o.i. For the separate system, both AdBC-VP2 and AdG5-FL were infected at the denoted m.o.i. The FL activities and GAL4-VP2 activator expression were examined at 48 h postinfection. Western blot analysis is shown at the bottom. The GAL4-VP2 activator was probed with anti-GAL4 polyclonal antibody (see Materials and Methods). β-Actin is shown as a control.

higher basal activity observed for the single virus AdTSTA-FL even in the presence of Casodex (Fig. 5).

Discussion

The key objectives of this study were to investigate the regulation of the TSTA system in different Ad configurations and to define the dynamic range of this system in different *in vivo* settings. Published and ongoing studies by our groups have demonstrated that TSTA technology is an effective approach to augment the activity of a weak tissue-specific promoter [27, 28]. Our goal is to develop these targeted gene expression systems for diagnostic and therapeutic applications in clinical settings. Thus, we have incorporated our PSA promoter-based TSTA system into an adenoviral gene delivery vector. Inserting the two components of TSTA, the activator and the reporter component, into a single vector does improve the functional efficiency of this system *in vivo*. In fact, the activity of the first single vector we generated, AdTSTA-FL, is quite impressive, as its activity consistently exceeded AdCMV-FL in all AR-expressing prostate cancer cell lines and tumors tested ([23] and this study), and it also displayed significant prostate specificity in cell culture studies, achieving 290-fold or higher levels of tissue discrimination (Fig. 2a). AR-mediated expression is a critical component of the PSA-based promoter in the TSTA system. We utilized the optical signal produced by AdTSTA-FL in tumors to monitor the dynamics of AR function during prostate cancer progression [23].

To understand the mechanism of activation of TSTA in adenoviral vectors better, we examined and compared the activity of single and separate TSTA configured Ads. The activity of this TSTA system is fully dependent on the GAL4-VP2 activator (Fig. 6). A second interesting finding is that despite equivalent promoter (PSE-BC) and gene delivery of the activator in the single and separate TSTA Ads, the single AdTSTA-FL consistently expressed an elevated level of GAL4-VP2 activator. This finding indicates that the head-to-head configuration in the single Ad promotes an increase in GAL4-VP2 and, hence, FL expression. This result could also contribute to the slightly elevated basal activity mediated by AdTSTA-FL in androgen-depleted cell culture medium. We hypothesize that a feedforward loop might be at play in the single AdTSTA-FL. A schematic illustration of this idea is shown in Fig. 7. The initial expression of GAL4-VP2 (step 1) is regulated by the PSE-BC promoter. In step 2, GAL4-VP2 binds to the GAL4 sites and activates FL gene expression. However, in the head-to-head configuration, the multiple GAL4-VP2 activators could also stimulate transcription in the direction of the PSE-BC promoter in an enhancer-like manner (step 3), further enhancing the synthesis of GAL4-VP2 (step 4). The feedforward loop leads to a perpetuating cycle of activator production that exceeds the natural capability of the PSE-BC promoter. This phenomenon could also contribute to "leaky" expression in nonprostate cells when the TSTA vector is administered at high m.o.i. From these results, we would postulate that functional separation of the activator and reporter components in a single vector might achieve tighter regulation of the TSTA system.

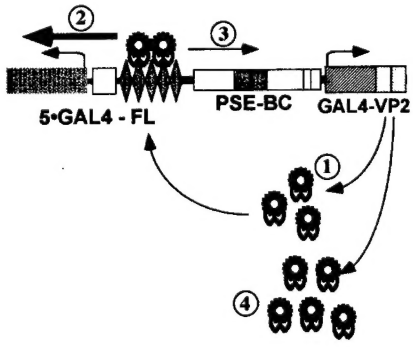

FIG. 7. Schematic representation of the activation mechanism and future designs of TSTA Ads. The feedforward loop mechanism postulates that GAL4-VP2 expression is upregulated by the activator's binding to the designed GAL4 sites in a self-activated manner.

ARTICLE

doi:10.1016/j.ymthe.2003.08.016

A transcriptionally targeted gene expression approach [reviewed in 45] could reduce the potential side effects of Ad-mediated cytotoxic cancer gene therapy such as that mediated by the herpes simplex virus thymidine kinase (HSV-TK) gene [46]. After intratumoral injection of Ad constitutively expressing luciferase or other reporter gene, leakage of the vector into systemic circulation resulted in transgene expression in the liver [26,47]. From this finding liver toxicity can be anticipated after intratumoral injection of CMV-driven HSV-TK Ad following administration of the prodrug ganciclovir. When a tissue- or cancer-specific promoter is employed to drive HSV-TK, the same extent of vector delivery to the liver is expected to occur. However, HSV-TK expression in the liver will be restricted by the tissue-specific promoter and therefore transgene-mediated liver toxicity should be reduced.

The gene-expression targeting approach employed in this study will not alter the *in vivo* liver distribution observed of Ad5 [26,48]. This preferential Ad transduction has contributed to liver toxicity [48–50] due to the innate immune response to viral capsid proteins [51] and cell-mediated immunity against viral gene products [52,53]. Utilization of a specific promoter to drive transgene expression was shown to reduce both the immune response against the Ad and the associated liver toxicity [54]. In addition, the potent gene expression mediated by the TSTA system could potentially reduce the amount of vector needed to transduce cancer cells *in vivo* compared to nonamplified tissue-specific vectors. Reducing the input dosage of Ad has been documented to reduce liver toxicity [49–52]. A second consequence of Ad sequestration in the liver [48,49] is that viral distribution to other organs such as kidney and intestine was nearly 1000-fold lower [55]. To improve *in vivo* gene transduction to other organs or tumors, many studies are under way to divert the natural adenovirus tropism away from the liver by ablation of CAR- and integrin-mediated interactions [48,55,56].

The inability to detect prostatic expression after tail vein administration of 10^7 pfu of AdTSTA-FL (Figs. 2b and 2c) could be due to liver sequestration. We have detected FL expression in the prostate after intravenous administration of 1.8×10^9 pfu of AdPSE-BC-FL [25]. The AdTSTA-FL is estimated to be about 50-fold more active than AdPSE-BC-FL [23,28]. However, the 180-fold lower dosage of AdTSTA-FL used in this study compared to AdPSE-BC-FL [25] might be below the threshold of detection for optical imaging. Moreover, by an intraperitoneal route of vector delivery we have been able to detect specific optical signals in the prostate (M. Johnson and L. Wu, unpublished data).

The mechanism for the low level of expression observed in lung tissue is unclear (Figs. 2b and 2c). We speculate that there could be transcription factors common to both lung and prostate that partially contribute to the regulation of the PSA promoter. For example, GATA zinc finger transcription factors have been shown to bind to the PSA promoter [57], and they are involved in lung development [58] and transcription of lung-specific promoters [59]. A large family of Ets transcription factors could also participate in epithelial-specific expression in the lung and prostate [60–62]. Investigating these intriguing possibilities might lead to a better understanding of tissue-specific gene regulation.

It is quite evident that the TSTA approach can amplify the activity of many other weak tissue-specific promoters. Dr. Gambhir's group has demonstrated that the activity of the hypoxia-inducible VEGF promoter can be amplified [63]. A similar approach has been employed to amplify the carcinoembryonic antigen promoter in a binary adenovirus system [64]. This approach exhibited increased therapeutic index compared to constitutive viral RSV-driven HSV-TK suicide gene therapy [64]. To adapt the TSTA system to other promoters, it will be necessary to adjust the various components of TSTA (i.e., the potency of the specific promoter, the strength of the activator, and the number of GAL4 sites) to achieve optimal regulation and expression dictated by the specific applications.

The modular and titratable nature of the TSTA system also makes it particularly attractive for a variety of gene therapy applications [28]. Transgene levels needed to achieve therapeutic efficacy in different gene therapy strategies might vary greatly; for example, p53 tumor suppressor expression in genetic corrective strategies might need to be higher than cytokine expression in immune-mediated tumor rejection. The various adjustable constituents of TSTA can be fine-tuned to achieve the most effective and least toxic therapeutic result. We have shown that transcriptionally targeted Ad (AdPSE-BC-luc) can achieve cell-specific expression to localize metastatic prostate cancer lesions in living mice, using optical CCD imaging [26]. To translate this finding to clinical diagnostic settings, a higher energy imaging modality will be needed to circumvent the loss of optical signal observed with increased tissue depth. Positron emission tomography (PET) is a radionuclide imaging modality widely used in clinical settings. Our institution has acquired substantial experience in adapting this modality to gene-based imaging in small animals, using the HSV-TK or the dopamine type 2 receptor reporter genes [29,30,65]. Compared to optical imaging, PET has the distinct advantage of providing tomographic quantitative image signals and adaptability for human imaging. However, optical imaging is several orders of magnitude higher in sensitivity than PET in small animal applications [66]. Thus, the highly amplified and prostate-specific expression mediated by TSTA will likely permit the development and successful implementation of gene-based PET imaging to detect metastasis *in vivo*.

Many of our studies have demonstrated that the TSTA system is a promising tool to create future targeted gene-based diagnostic and therapeutic applications. With an

doi:10.1016/j.ymthe.2003.08.016

ARTICLE

in-depth understanding of its functional properties and fine-tuning of various components of TSTA, a truly safe, effective, and specific treatment can be developed for metastatic or hormone-refractory prostate cancer.

MATERIALS AND METHODS

Adenovirus constructs. AdCMV-FL was constructed as previously described [25,33]. The single AdTSTA-FL and separate TSTA Ads, AdBC-VP2 and AdG5-FL, were constructed with the AdEasy system [35]. The head-to-head fragment of activator and reporter in the single virus was derived from PBCVP2G5-L [28]. The construction of AdTSTA-FL has been previously described [23]. A *NotI* fragment containing the PSE-BC-driven GAL4-VP2 expression cassette was cloned into the *NotI* site of pShuttle to generate AdBC-VP2. For the construction of AdG5-FL, an *Asp718–SalI* fragment with five GAL4 binding sites upstream of the minimal adenovirus E4 and FL genes was blunted and ligated into the *Eco*RV site of pShuttle. All the pShuttle expression plasmids were used for recombination with pAdEasy-1 in the BJ5183 rec^+ bacteria strain to generate the full-length recombinant virus-containing plasmid. The viruses were propagated in 293 cells, purified on a CsCl gradient, and titered by plaque assays on 293 monolayers. Viruses are stored in 10 mM Tris–HCl, 1 mM $MgCl_2$, and 10% glycerol at −80°C until use.

Cell culture and infection studies. The human prostate cancer cell lines, LNCaP and LAPC-4, were grown in RPMI 1640 and Iscove's modified DMEM, respectively, and supplemented with 10% fetal bovine serum (FBS) and 1% penicillin/streptomycin solution. PC-3, Du145, HeLa, MCF7, HepG2, A549, and H157 cells were cultured in RPMI 1640 (Mediatech, Herndon, VA) with 10% FBS and 1% penicillin/streptomycin. For FL assays, the cultured cells were plated onto 24-well plates at 5×10^4 cells per well, and cells were counted at the day of infection to calculate m.o.i. For prostate cell lines, medium was replaced with 10% charcoal-stripped serum for 2 days prior to infection. The cells were infected with AdTSTA-FL or co-infected with AdBC-VP2 and AdG5-FL at certain m.o.i. Following infection, the synthetic androgen methylenetrienolone (R1881; NEN Life Science Products, Boston, MA) or anti-androgen bicalutamide (Casodex) was added to samples as indicated. At 48 h postinfection, the cells were harvested and lysed, using passive lysis buffer (Promega, Madison, WI). Levels of FL activity were measured according to the manufacturer's instructions (Promega), using a luminometer (Berthold Detection Systems, Pforzheim, Germany) with a 10-s integration time. Each value was calculated as the average of triplicate samples.

Real-time PCR was performed to quantify the amount of intracellular viral DNA. HeLa, MCF7, HepG2, H157, A549, and LNCaP cells were infected with AdG5-FL at m.o.i. 0.1 or 1 36 h after plating. After 12 h, cells were harvested and lysed. The total DNA was prepared with the DNeasy Tissue Kit (Qiagen, Valencia, CA). Opticon2 (MJ Research, Boston, MA) real-time PCR was performed, using these DNAs as template and the DyNAmo SYBR Green qPCR Kit (Finnzymes, Espoo, Finland). The viral FL sequences were detected by the following primer set: FL-a (5′-GAGATACGCCCTGGTTCCTG-3′) and FL-b (5′-GCATACGACGATTCTGTGATTTG-3′). Infectivity was calculated based on the copy number of internalized viral DNA divided by cell number. The relative infectivities of all cells are in reference to HeLa cells, which were set as 1, as they are the least susceptible to infection among the cell lines we tested.

Animal experiments with CCD imaging. Animal care and procedures were performed in accordance with the University of California Animal Research Committee guidelines. Eight- to ten-week-old male SCID mice (ICRSC-M, ~25 g, Taconic Farms, Germantown, NY) were used in these studies. Human prostate tumor xenografts were generated in SCID mice as previously described [41]. The LAPC-4 xenograft was originally provided by Dr. Charles Sawyers at UCLA. We passaged the tumor by implanting small tumor fragments mixed 1:1 with Matrigel (Collaborative Research, Bedford, MA) subcutaneously into the flanks of male SCID mice.

For the naïve mouse experiments, 10^7 pfu of Ad was injected via the tail vein ($n = 3$). *In vivo* expression was monitored sequentially over time. For the LAPC-4 xenografts, tumors were allowed to grow for 3 weeks prior to injection and reached a diameter of approximately 1 cm. AdBC-VP2 and AdG5-FL (10^8 pfu each) or AdTSTA-FL (10^7 pfu) was injected at three sites on each tumor at 10 μl per site ($n = 3$). Optical CCD imaging was performed at the indicated days postinjection. Intraprostatic injections were performed 7 days after castration. Both castrated and noncastrated animals received injection of 10^8 infectious units each of the paired TSTA Ads or 10^6 infectious units of the single TSTA Ad in both posterior lobes of the prostate ($n = 4$ per group). For each imaging session, the mice were anesthetized with ketamine/xylazine (4:1), and the d-luciferin substrate (150 mg/kg in PBS, Xenogen) was given intraperitoneally at a volume of 200 μl, with a 20-min incubation period prior to imaging. CCD images were obtained using a cooled IVIS CCD camera (Xenogen, Alameda, CA), and images were analyzed with IGOR-PRO Living Image Software, as described [26,28], in units of photons acquired per second per square centimeter per steridan.

Western blot analysis of GAL4-VP2 expression. LNCaP cells were grown in 60-mm dishes and infected with AdTSTA-FL or co-infected with AdBC-VP2 and AdG5-FL at m.o.i. 0.21, 0.62, 1.9, 5.6, 16.7, or 50 (threefold serial dilution). For co-infection, each Ad was administered at the m.o.i. listed above. Forty-eight hours later, the cells were harvested and lysed with RIPA buffer (1% NP-40, 0.1% sodium deoxycholate, 150 mM NaCl, and 50 mM Tris–HCl (pH 7.5), protease inhibitor cocktail (Sigma, St. Louis, MO)). The samples were fractionated on 8–16% gradient acrylamide gels (Gradipore, Frenchs Forest, Australia) and subjected to immunoblot analysis with rabbit polyclonal antibodies generated against intact GAL4-VP2 or β-actin A5316 (Sigma). Detection was done by visualization of bands with HRP-labeled secondary antibody and ECL (Amersham Pharmacia Biotech, Piscataway, NJ).

ACKNOWLEDGMENTS

We appreciate the technical support of Erika Billick, the assistance of Wendy Aft on manuscript preparation, and helpful discussions with Drs. Harvey Herschman and Helen Brown. This work is supported by Department of Defense (DOD) CDMRP PC020536 (to L.W.), California Cancer Research Program 3NI0226 (to L.W.), NIH R01 CA101904 (to L.W.), CapCURE (to M.C., S.S.G.), DOD PC 991019 (to Charles Sawyers and M.C.), DOD PC020177 (to M.C.), an interdisciplinary seed grant from the JCCC (to M.C., L.W., and S.S.G.), R01 CA82214 (to S.S.G.), SAIRP R24 CA92865 (to S.S.G.), and Department of Energy Contract DE-FC03-87ER60615 (to S.S.G.). M.S. is supported by a DOD CDMRP postdoctoral fellowship (PC020531).

RECEIVED FOR PUBLICATION JUNE 16; ACCEPTED AUGUST 20, 2003.

REFERENCES

1. American Cancer Society (2002). Cancer Facts & Figures 2002. Am. Cancer Soc., Atlanta, pp. 3–15.
2. Denis, L., and Murphy, G. P. (1993). Overview of phase III trials on combined androgen treatment in patients with metastatic prostate cancer. *Cancer* **72:** 3888–3895.
3. Hellerstedt, B. A., and Pienta, K. J. (2002). The current state of hormonal therapy for prostate cancer. *CA Cancer J. Clin.* **52:** 154–179.
4. Labrie, F. (2002). Androgen blockade in prostate cancer in 2002: major benefits on survival in localized disease. *Mol. Cell. Endocrinol.* **198:** 77–87.
5. Mabjeesh, N. J., Zhong, H., and Simons, J. W. (2002). Gene therapy of prostate cancer: current and future directions. *Endocr. Relat. Cancer* **9:** 115–139.
6. Wu, L. and Sato, M. (2003). Integrated, molecular engineering approaches to develop prostate cancer gene therapy. *Curr. Gene Ther.* (in press).
7. Cleutjens, K. B., van der Korput, H. A., van Eekelen, C. C., van Rooij, H. C., Faber, P. W., and Trapman, J. (1997). An androgen response element in a far upstream enhancer region is essential for high, androgen-regulated activity of the prostate-specific antigen promoter. *Mol. Endocrinol.* **11:** 148–161.
8. Noss, K. R., Wolfe, S. A., and Grimes, S. R. (2002). Upregulation of prostate specific membrane antigen/folate hydrolase transcription by an enhancer. *Gene* **285:** 247–256.
9. O'Keefe, D. S., *et al.* (1998). Mapping, genomic organization and promoter analysis of the human prostate-specific membrane antigen gene. *Biochim. Biophys. Acta* **1443:** 113–127.
10. Pang, S., *et al.* (1997). Identification of a positive regulatory element responsible for tissue-specific expression of prostate-specific antigen. *Cancer Res.* **57:** 495–499.

AQ: 1

ARTICLE

doi:10.1016/j.ymthe.2003.08.016

11. Schuur, E. R., Henderson, G. A., Kmetec, L. A., Miller, J. D., Lamparski, H. G., and Henderson, D. R. (1996). Prostate-specific antigen expression is regulated by an upstream enhancer. *J. Biol. Chem.* **271:** 7043–7051.
12. Watt, F., *et al.* (2001). A tissue-specific enhancer of the prostate-specific membrane antigen gene, FOLH1. *Genomics* **73:** 243–254.
13. Hobisch, A., Culig, Z., Radmayr, C., Bartsch, G., Klocker, H., and Hittmair, A. (1995). Distant metastases from prostatic carcinoma express androgen receptor protein. *Cancer Res.* **55:** 3068–3072.
14. Koivisto, P. A., and Helin, H. J. (1999). Androgen receptor gene amplification increases tissue PSA protein expression in hormone-refractory prostate carcinoma. *J. Pathol.* **189:** 219–223.
15. Sweat, S. D., Pacelli, A., Bergstralh, E. J., Slezak, J. M., Cheng, L., and Bostwick, D. G. (1999). Androgen receptor expression in prostate cancer lymph node metastases is predictive of outcome after surgery. *J. Urol.* **161:** 1233–1237.
16. van der Kwast, T. H., and Tetu, B. (1996). Androgen receptors in untreated and treated prostatic intraepithelial neoplasia. *Eur. Urol.* **30:** 265–268.
17. Bok, R. A., and Small, E. J. (2002). Bloodborne biomolecular markers in prostate cancer development and progression. *Nat. Rev. Cancer* **2:** 918–926.
18. Feldman, B. J., and Feldman, D. (2001). The development of androgen-independent prostate cancer. *Nat. Rev. Cancer* **1:** 34–45.
19. Visakorpi, T., *et al.* (1995). In vivo amplification of the androgen receptor gene and progression of human prostate cancer. *Nat. Genet.* **9:** 401–406.
20. Gregory, C. W., *et al.* (2001). A mechanism for androgen receptor-mediated prostate cancer recurrence after androgen deprivation therapy. *Cancer Res.* **61:** 4315–4319.
21. Zhou, Z. X., Lane, M. V., Kemppainen, J. A., French, F. S., and Wilson, E. M. (1995). Specificity of ligand-dependent androgen receptor stabilization: receptor domain interactions influence ligand dissociation and receptor stability. *Mol. Endocrinol.* **9:** 208–218.
22. Abreu-Martin, M. T., Chari, A., Palladino, A. A., Craft, N. A., and Sawyers, C. L. (1999). Mitogen-activated protein kinase kinase kinase 1 activates androgen receptor-dependent transcription and apoptosis in prostate cancer. *Mol. Cell. Biol.* **19:** 5143–5154.
23. Zhang, L., *et al.* (2003). Interrogating androgen receptor function in recurrent prostate cancer. *Cancer Res.* (in press). AQ: 2
24. Latham, J. P., Searle, P. F., Mautner, V., and James, N. D. (2000). Prostate-specific antigen promoter/enhancer driven gene therapy for prostate cancer: construction and testing of a tissue-specific adenovirus vector. *Cancer Res.* **60:** 334–341.
25. Wu, L., *et al.* (2001). Chimeric PSA enhancers exhibit augmented activity in prostate cancer gene therapy vectors. *Gene Ther.* **8:** 1416–1426.
26. Adams, J. Y., *et al.* (2002). Visualization of advanced human prostate cancer lesions in living mice by a targeted gene transfer vector and optical imaging. *Nat. Med.* **8:** 891–897.
27. Iyer, M., Wu, L., Carey, M., Wang, Y., Smallwood, A., and Gambhir, S. S. (2001). Two-step transcriptional amplification as a method for imaging reporter gene expression using weak promoters. *Proc. Natl. Acad. Sci. USA* **98:** 14595–14600.
28. Zhang, L., *et al.* (2002). Molecular engineering of a two-step transcription amplification (TSTA) system for transgene delivery in prostate cancer. *Mol. Ther.* **5:** 223–232.
29. Blasberg, R. G., and Tjuvajev, J. G. (1999). Herpes simplex virus thymidine kinase as a marker/reporter gene for PET imaging of gene therapy. *Q. J. Nucl. Med.* **43:** 163–169.
30. Gambhir, S. S. (2002). Molecular imaging of cancer with positron emission tomography. *Nat. Rev. Cancer* **2:** 683–693.
31. Massoud, T., and Gambhir, S. S. (2003). Molecular imaging in living subjects: seeing fundamental biological processes in a new light. *Genes Dev.* **17:** 545–580.
32. Rehemtulla, A., *et al.* (2000). Rapid and quantitative assessment of cancer treatment response using in vivo bioluminescence imaging. *Neoplasia* **2:** 491–495.
33. Wu, J. C., Sundaresan, G., Iyer, M., and Gambhir, S. S. (2001). Noninvasive optical imaging of firefly luciferase reporter gene expression in skeletal muscles of living mice. *Mol. Ther.* **4:** 297–306.
34. Ciana, P., *et al.* (2003). In vivo imaging of transcriptionally active estrogen receptors. *Nat. Med.* **9:** 82–86.
35. He, T. C., Zhou, S., da Costa, L. T., Yu, J., Kinzler, K. W., and Vogelstein, B. (1998). A simplified system for generating recombinant adenoviruses. *Proc. Natl. Acad. Sci. USA* **95:** 2509–2514.
36. Bergelson, J. M., *et al.* (1997). Isolation of a common receptor for coxsackie B viruses and adenoviruses 2 and 5. *Science* **275:** 1320–1323.
37. Roelvink, P. W., Mi Lee, G., Einfeld, D. A., Kovesdi, I., and Wickham, T. J. (1999). Identification of a conserved receptor-binding site on the fiber proteins of CAR-recognizing adenoviridae. *Science* **286:** 1568–1571.
38. Wickham, T. J., Mathias, P., Cheresh, D. A., and Nemerow, G. R. (1993). Integrins alpha v beta 3 and alpha v beta 5 promote adenovirus internalization but not virus attachment. *Cell* **73:** 309–319.
39. Fechner, H., *et al.* (2000). Trans-complementation of vector replication versus coxsackie–adenovirus-receptor overexpression to improve transgene expression in poorly permissive cancer cells. *Gene Ther.* **7:** 1954–1968.
40. Rauen, K. A., *et al.* (2002). Expression of the coxsackie adenovirus receptor in normal prostate and in primary and metastatic prostate carcinoma: potential relevance to gene therapy. *Cancer Res.* **62:** 3812–3818.
41. Klein, K. A., *et al.* (1997). Progression of metastatic human prostate cancer to androgen independence in immunodeficient SCID mice. *Nat. Med.* **3:** 402–408.
42. Fechner, H., *et al.* (1999). Expression of coxsackie adenovirus receptor and alphav-integrin does not correlate with adenovector targeting in vivo indicating anatomical vector barriers. *Gene Ther.* **6:** 1520–1535.
43. Kijima, T., *et al.* (1999). Application of the Cre recombinase/loxP system further enhances antitumor effects in cell type-specific gene therapy against carcinoembryonic antigen-producing cancer. *Cancer Res.* **59:** 4906–4911.
44. Ueda, K., *et al.* (2001). Carcinoembryonic antigen-specific suicide gene therapy of cytosine deaminase/5-fluorocytosine enhanced by the Cre/loxP system in the orthotopic gastric carcinoma model. *Cancer Res.* **61:** 6158–6162.
45. Wu, L., Johnson, M. and Sato, M. (2003). Transcriptionally-targeted gene therapy to detect and treat cancer. *Trends Mol. Med.* (in press). AQ: 3
46. Shalev, M., *et al.* (2000). Suicide gene therapy toxicity after multiple and repeat injections in patients with localized prostate cancer. *J. Urol.* **163:** 1747–1750.
47. Lohr, F., Huang, Q., Hu, K., Dewhirst, M. W., and Li, C. Y. (2001). Systemic vector leakage and transgene expression by intratumorally injected recombinant adenovirus vectors. *Clin. Cancer Res.* **7:** 3625–3628.
48. Alemany, R., and Curiel, D. T. (2001). CAR-binding ablation does not change biodistribution and toxicity of adenoviral vectors. *Gene Ther.* **8:** 1347–1353.
49. Tao, N., *et al.* (2001). Sequestration of adenoviral vector by Kupffer cells leads to a nonlinear dose response of transduction in liver. *Mol. Ther.* **3:** 28–35.
50. Morral, N., *et al.* (2002). Lethal toxicity, severe endothelial injury, and a threshold effect with high doses of an adenoviral vector in baboons. *Hum. Gene Ther.* **13:** 143–154.
51. Zhang, Y., *et al.* (2001). Acute cytokine response to systemic adenoviral vectors in mice is mediated by dendritic cells and macrophages. *Mol. Ther.* **3:** 697–707.
52. Yang, Y., Su, Q., and Wilson, J. M. (1996). Role of viral antigens in destructive cellular immune responses to adenovirus vector-transduced cells in mouse lungs. *J. Virol.* **70:** 7209–7212.
53. Jooss, K., Yang, Y., Fisher, K. J., and Wilson, J. M. (1998). Transduction of dendritic cells by DNA viral vectors directs the immune response to transgene products in muscle fibers. *J. Virol.* **72:** 4212–4223.
54. Pastore, L., *et al.* (1999). Use of a liver-specific promoter reduces immune response to the transgene in Ads. *Hum. Gene Ther.* **10:** 1773–1781.
55. Nakamura, T., Sato, K., and Hamada, H. (2003). Reduction of natural adenovirus tropism to the liver by both ablation of fiber-coxsackievirus and adenovirus receptor interaction and use of replaceable short fiber. *J. Virol.* **77:** 2512–2521.
56. Einfeld, D. A., *et al.* (2001). Reducing the native tropism of adenovirus vectors requires removal of both CAR and integrin interactions. *J. Virol.* **75:** 11284–11291.
57. Perez-Stable, C. M., Pozas, A., and Roos, B. A. (2000). A role for GATA transcription factors in the androgen regulation of the prostate-specific antigen gene enhancer. *Mol. Cell. Endocrinol.* **167:** 43–53.
58. Laverriere, A. C., MacNeill, C., Mueller, C., Poelmann, R. E., Burch, J. B., and Evans, T. (1994). GATA-4/5/6, a subfamily of three transcription factors transcribed in developing heart and gut. *J. Biol. Chem.* **269:** 23177–23184.
59. Bruno, M. D., Korfhagen, T. R., Liu, C., Morrisey, E. E., and Whitsett, J. A. (2000). GATA-6 activates transcription of surfactant protein A. *J. Biol. Chem.* **275:** 1043–1049.
60. Neve, R., *et al.* (1998). The epithelium-specific ets transcription factor ESX is associated with mammary gland development and involution. *FASEB J.* **12:** 1541–1550.
61. Oettgen, P., *et al.* (2000). PDEF, a novel prostate epithelium-specific ets transcription factor, interacts with the androgen receptor and activates prostate-specific antigen gene expression. *J. Biol. Chem.* **275:** 1216–1225.
62. Tymms, M. J., *et al.* (1997). A novel epithelial-expressed ETS gene, ELF3: human and murine cDNA sequences, murine genomic organization, human mapping to 1q32.2 and expression in tissues and cancer. *Oncogene* **15:** 2449–2462.
63. Wang, Y., Iyer, M., Wu, L., Carey, M., and Gambhir, S. S. (2002). A two-step transcriptional approach for imaging of vascular endothelial growth factor (VEGF) gene expression using a bioluminescent reporter gene. *Mol. Imaging Biol.* **4:** S42.
64. Qiao, J., *et al.* (2002). Tumor-specific transcriptional targeting of suicide gene therapy. *Gene Ther.* **9:** 168–175.
65. Gambhir, S. S., *et al.* (2000). Imaging transgene expression with radionuclide imaging technologies. *Neoplasia* **2:** 118–138.
66. Ray, P., Wu, A. M., and Gambhir, S. S. (2003). Optical bioluminescence and positron emission tomography imaging of a novel fusion reporter gene in tumor xenografts of living mice. *Cancer Res.* **63:** 1160–1165.